

GNSS TEC-Based Detection and Analysis of Acoustic-Gravity Waves From the 2012 Sumatra Double Earthquake Sequence

Sarthak Srivastava, Amal Chandran, Fabio Manta, Benoit Taisne

▶ **To cite this version:**

Sarthak Srivastava, Amal Chandran, Fabio Manta, Benoit Taisne. GNSS TEC-Based Detection and Analysis of Acoustic-Gravity Waves From the 2012 Sumatra Double Earthquake Sequence. Journal of Geophysical Research Space Physics, 2021, 126, p.382-401. 10.1029/2020JA028507 . insu-03590045

HAL Id: insu-03590045

https://insu.hal.science/insu-03590045

Submitted on 3 Mar 2022

HAL is a multi-disciplinary open access archive for the deposit and dissemination of scientific research documents, whether they are published or not. The documents may come from teaching and research institutions in France or abroad, or from public or private research centers.

L'archive ouverte pluridisciplinaire **HAL**, est destinée au dépôt et à la diffusion de documents scientifiques de niveau recherche, publiés ou non, émanant des établissements d'enseignement et de recherche français ou étrangers, des laboratoires publics ou privés.

Copyright

Check for updates

Tectonics

RESEARCH ARTICLE
10.1029/2020TC006567

Key Points:

- The Kumawa fault has greatly deformed the Banda forearc to generate prominent seafloor expression and cut through the entire upper plate
- The fault is mainly formed by the forearc extension induced by the subduction rollback of the Banda slab during the last 2 Ma
- It has a reduced slip rate from 40 mm/yr (geological rate) to <14 mm/yr (geodetic rate), and is partially locked awaiting a large event

Correspondence to:
X. Yang,
yang@ipgp.fr

Citation:
Yang, X., Singh, S. C., & Deighton, I. (2021). The margin-oblique Kumawa strike-slip fault in the Banda forearc, East Indonesia: Structural deformation, tectonic origin and geohazard implication. *Tectonics*, *40*, e2020TC006567. https://doi.org/10.1029/2020TC006567

Received 8 OCT 2020
Accepted 8 MAR 2021

© 2021. American Geophysical Union. All Rights Reserved.

The Margin-Oblique Kumawa Strike-Slip Fault in the Banda Forearc, East Indonesia: Structural Deformation, Tectonic Origin and Geohazard Implication

Xiaodong Yang[1], Satish C. Singh[1], and Ian Deighton[2]

[1]Université de Paris, Institut de physique du globe de Paris, CNRS, Paris, France, [2]TGS, Surbiton, UK

Abstract The northeast Banda margin is affected by the arc-continent collision between the Australian continental margin and the Banda arc. Unlike margin-parallel strike-slip faults in other subduction zones, the margin-oblique Seram-Kumawa Shear Zone (SKSZ) has greatly deformed the Banda forearc with 80 km displacement along plate boundary. It trends ~ WNW-ESE comprising the Kawa shear zone (KSZ, >200 km) on the Seram island and the Kumawa fault (KF, >200 km) offshore SE Seram. Using multibeam bathymetry, marine seismic reflection and earthquake data, we studied the active tectonics and driving mechanism of the SKSZ with focus on its offshore part (KF). Our results show: (1) the KF is a young (~2 Ma), linear crustal structure with three segments from NW to SE: pull-apart basin (dextral), diffuse shear zone (sinistral) and distinct fault trace (sinistral); (2) It propagates southeastward and cross-cuts the entire upper plate with prominent seafloor expression, but without seismicity along it, similar to the Banda detachment caused by forearc extension; (3) By incorporating the oblique collision and regional tectonics with our results, we proposed that the KF is formed primarily by the upper plate extension induced by subduction rollback during the last 2 Ma, with minor contribution from oblique arc-continent collision; (4) The slip rate of the KF has reduced from 40 mm/yr over 2 Ma to <14 mm/yr at present. These observations combined with the clear seafloor faulting, 80-km displacement and occurrence of a Mw 5.2 earthquake on its horsetail fault suggest it is currently locked awaiting a large earthquake.

1. Introduction

An oceanic plate subduction along active margins is often accompanied by oblique convergence with obliquity increasing away from the subduction center (Philippon & Corti, 2016), for example, Banda, Sumatra, Caribbean, Marianas, Hikurangi, Alentian, Hellenic, etc. The slip vector oblique to such margins is partitioned into a dip-slip, the orthogonal component, responsible for under-thrusting in the subduction zones and a strike-slip component responsible for transcurrent motions parallel to the margin on the upper plate (Fitch, 1972; McCaffrey, 1992; Schütt & Whipp, 2020). Examples of such large transcurrent strike-slip faults include the Great Sumatra Fault in Sunda (e.g., McCaffrey, 2009), the Enriquillo Plaintain Garden fault (EPGF) in Caribbean (e.g., Calais et al., 1992; Mann et al., 1995), and the Alpine fault in New Zealand (e.g., Norris & Cooper, 2001). These faults are mostly on the overriding plate, close to volcanic arcs (Manaker et al., 2008) with length up to several hundred kilometers or more. To our knowledge, there is no such fault system on both upper and lower plates. These strike-slip faults are prone to generate large earthquakes, for example, the 2010 Haiti Mw 7.1 earthquake on the EPGF (Calais et al., 2010). A few of them have been the locus of a series of scientific investigation in the recent past (e.g., GSF, Ghosal et al., 2012; McCaffrey, 1992; Sieh & Natawidjaja, 2000). However, the scarce bathymetry and/or marine seismic data used previously only covers part of these faults. To better understand the active tectonics and geohazards of such large, disastrous fault system on plate margins, a high-resolution topography/bathymetry map combined with marine seismic data along the entire fault is required, which is rarely available. Furthermore, all these fault systems seem to mainly affect the upper plate. Here, we study a fault system that was suggested to have affected both the upper and lower plates in the Banda arc region.

The Banda arc is situated in the eastern Indonesia where a complex convergence is taking place between the Australia, Eurasia, Pacific and Philippine Sea plates (e.g., Charlton, 2010; DeMets et al., 1994; Hall, 1996, 2012; Hamilton, 1979; Hinschberger et al., 2005), with both contraction and extension accompanied by subduction hinge rollback, lithospheric delamination and slab break off (e.g., Harris, 1992;

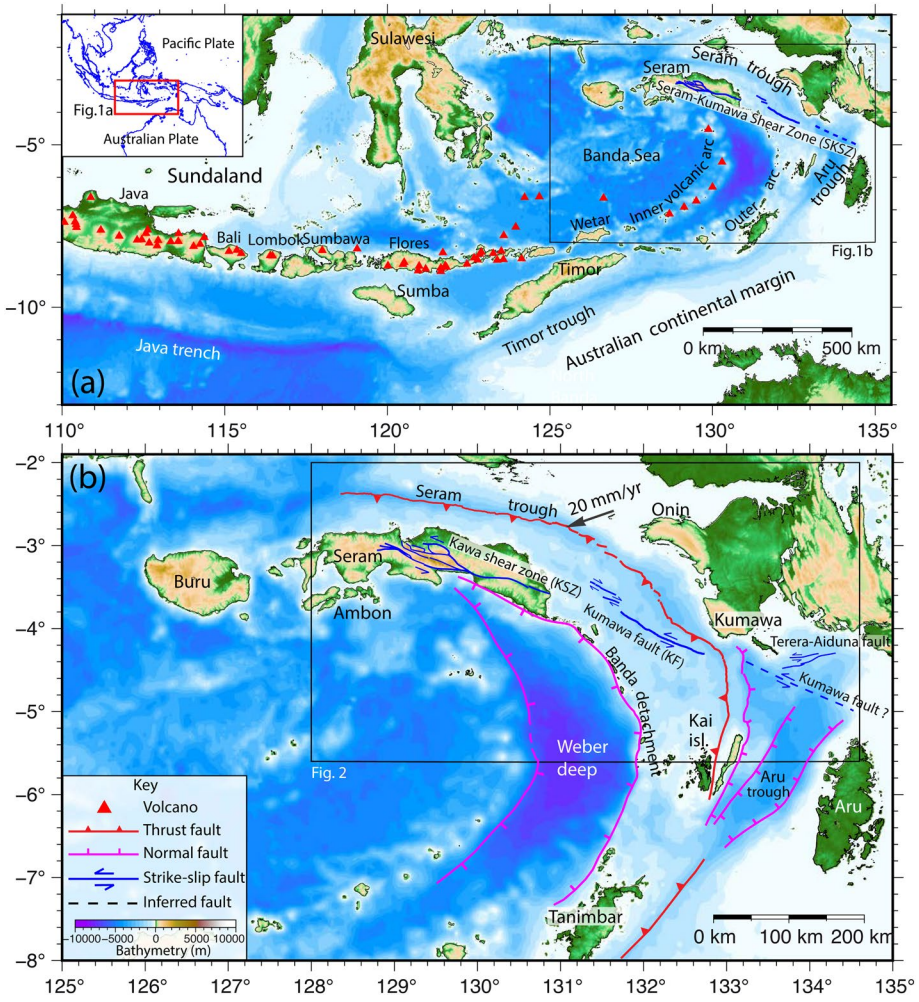


Figure 1. Regional map of the study area. (a) The Sunda-Banda subduction-collision system in east Indonesia. (b) Tectonic map of the east Banda arc region. Structural features modified from Hinschberger et al. (2003), Pownall et al. (2016) and Hall et al. (2017). Topography and bathymetry are from Global ocean & land terrain models (https://www.gebco.net). The 20 mm/yr rate of plate convergence between the Australian continental margin and the Banda arc is taken from Bock et al. (2003).

Hall, 2012; Spakman & Hall, 2010). The spectacularly curved Banda arc comprises young oceanic crust enclosed by a volcanic inner arc, outer arc islands and a trough (i.e., Seram trough) parallel to the Australian continental margin (Figure 1a; Bowin et al., 1980; Hall & Spakman, 2015; Hamilton, 1979; Hinschberger et al., 2001; Spakman & Hall, 2010). Along the Seram trough, the Australian continental margin is obliquely colliding with the Banda arc at a rate of 20 mm/yr (Figure 1b; Bock et al., 2003; Simons et al., 2007). A series of WNW-ESE trending strike-slip faults and shear zones have developed within the Banda forearc (Figure 1b), such as the 200-km-long Kawa shear zone (KSZ) on Seram (Pownall et al., 2013, 2014; Watkinson & Hall, 2017), the proposed >400-km-long Kumawa fault (KF) offshore SE Seram and north of the Aru trough (Figure 1; Adhitama et al., 2017; Hall et al., 2017; Patria & Hall, 2017). They are predominantly sinistral strike-slip faults but in places with evidence of dextral motion (Pownall et al., 2013; Watkinson & Hall, 2017). Hall et al. (2017) suggested that all these faults are linked to be an important regional structure, namely the Seram-Kumawa Shear Zone (SKSZ; Figures 1a and 1b). Despite being similar to other strike-slip faults in the oblique subduction complex, a few features of the SKSZ appear to be peculiar: (1) it seems to be segmented, that is, into the onshore KSZ and offshore KF; (2) it is oblique to the margin and has caused a large displacement (80 km) along the Seram trough (Hall et al., 2017; this study); (3) there is no major seismicity associated with its offshore portion along the KF; (4) the SKSZ seems to have deformed both the

upper and lower plates (Hall et al., 2017), in contrast to other strike-slip faults in subduction zones (e.g., Calais et al., 1992; McCaffrey, 1992; Schütt & Whipp, 2020). These unique features make the origin, structure, tectonics and geodynamics of such fault system intriguing.

Based on high-resolution bathymetry, onshore topography, marine seismic reflection and earthquake data, here we shed light on the tectonic evolution of the SKSZ with focus on its offshore portion, that is, the Kumawa fault, in the geodynamic context of an active margin that has undergone a past oceanic subduction, subduction roll-back and ongoing oblique arc-continent collision (Hall, 2012, 2017; Spakman & Hall, 2010). We first concentrate on the geometry, structure and spatial distribution of the entire SKSZ in the northeast Banda. We then analyze its timing, segmentation, displacement, slip rate and seismicity. Finally, we will discuss its geohazard potential and its role in the regional geodynamics of the east Banda margin.

2. Datasets and Methods

In 2007/2008, a multi-client geophysical company TGS acquired substantial multi-beam bathymetry data in the east Seram region and in the north Aru trough (Figure 2a). The bathymetry data have been used to study the extensional tectonics in the Aru trough and the structural variation along the Seram trough (Adhitama et al., 2017; Hall et al., 2017; Patria & Hall, 2017). The high-resolution 2-D marine seismic profiles were collected by TGS in 1997–1998 and 2007–2008. We do not have the acquisition details for the 1997–1998 data. The 2007–2008 data was acquired on board a seismic vessel towing a 7-km-long streamer at 7.0 m water depth and a 3,940 in^3 airgun source towed at 5 m depth. The shot point interval was 25 m, and the record length was 8.0 s. It was processed using a standard processing technique that includes noise suppression, common-mid point binning, velocity analysis, and pre-stack time migration. Special attention was given to enhance the low frequencies. Earthquakes presented in this study are from the catalog of Global Centroid Moment Tensor (GCMT, Mw > 5), https://www.globalcmt.org/CMTsearch.html.

Key methods used in study include structural mapping, seismic interpretation, construction of topography and earthquake profiles, fault analysis, displacement measurements, and creation of 3D bathymetry models.

3. Regional Tectonics

The east Banda margin represents a unique example of arc-continent collision and one of the most tectonically complex and seismically active areas on Earth (Michel et al., 2001; Puntodewo et al., 1994). As the most remarkable feature in the region, the Banda arc is famous for its 180° curvature in Benioff zone contours (Spakman & Hall, 2010, Figure 1). Two tectonic models have previously been proposed to explain this curvature: (1) one single slab that was deformed in the mantle (e.g., Audley-Charles, 1975; Hall, 1996, 2002; Hamilton, 1979; Milsom, 2001; Spakman & Hall, 2010); (2) two separate slabs sub-ducted from the north and south, respectively (e.g., Bowin et al., 1980; Cardwell & Isacks, 1978; Das, 2004; Hinschberger et al., 2005; McCaffrey, 1989; Špičák & Vaněk, 2013). This argument has now been well addressed in favor of the single slab model (Hall, 2012; Spakman & Hall, 2010), and the curvature is interpreted to result from the southeastward rollback of the sub-ducting oceanic lithosphere of the Proto-Banda Sea Plate into a pre-existing *U*-shaped oceanic Banda embayment at the Australian continental margin at 16 Ma (Hall, 2012; Hall & Spakman, 2015; Spakman & Hall, 2010).

The islands of the Banda Arc are composed of an inner volcanic arc and an outer non-volcanic arc in which the largest islands are Timor in the south and Seram in the north (Hall et al., 2017, Figure 1a). The inner volcanic arc has been active since the Late Miocene (11 Ma, Abbott & Chamalaun, 1981; Barberi et al., 1987; Honthaas et al., 1998) and the outer arc is widely regarded as a result of the recent collision between the Australian continental margin and the Banda volcanic arc (Figure 1) and has been uplifted rapidly since the mid Pliocene (Pairault et al., 2003). This collision has also caused the formation of the Seram fold-thrust belt (SFTB) at the Banda forearc since 3.6 Ma (Pairault et al., 2003; Spakman & Hall, 2010). About 150 km north of the Seram island, a deep bathymetric trough, the arc-shaped Seram trough, runs for ~2,000 km and links with the Timor trough in the south, and ultimately connects with the Java trench in the west (Figure 1a).

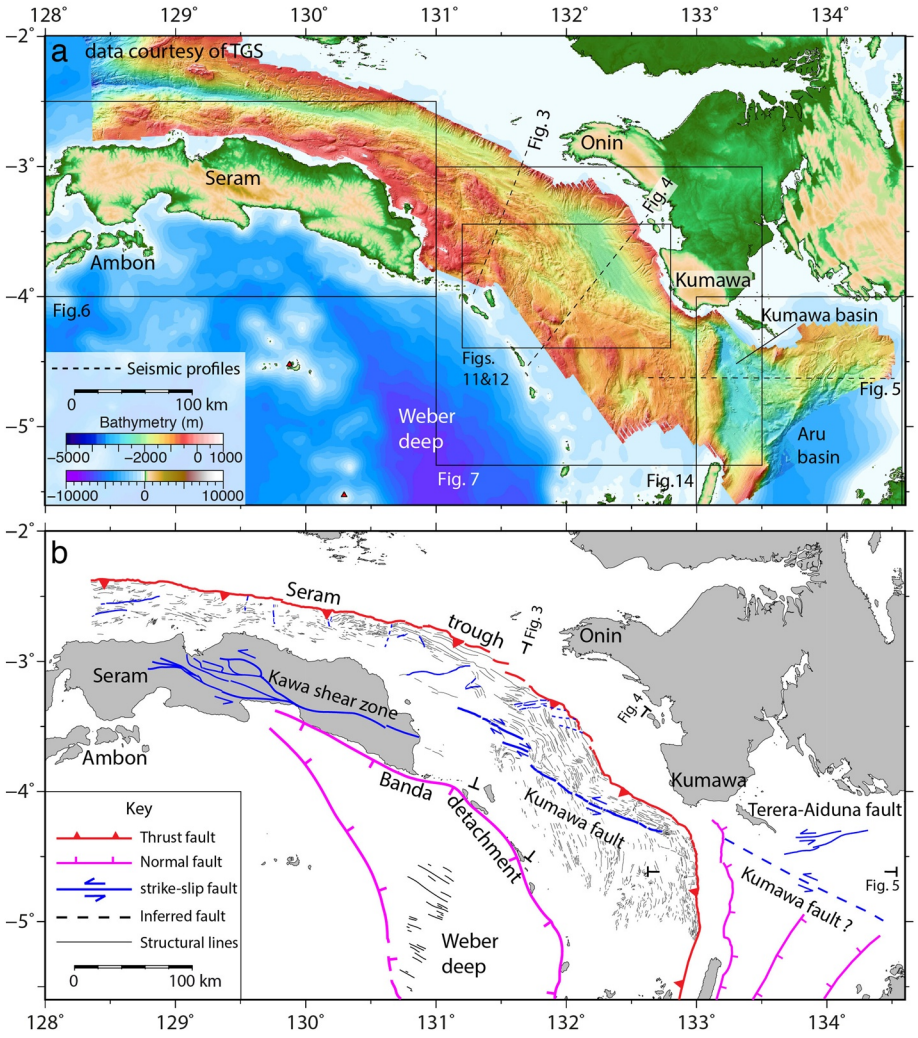


Figure 2. Detailed structural mapping on the east Banda margin using high-resolution bathymetry and topography. (a) A combination of 25-m resolution and 100-m resolution bathymetry showing the base map. (b) Result of structural mapping. For location of the map see Figure 1b.

It is interpreted as a fore deep produced by the loading of the newly developed SFTB (Pairault et al., 2003; Spakman & Hall, 2010). The arc-continent collision has also led to intense shallow seismicity generated by active thrust faulting (Bock et al., 2003; McCaffrey, 1989) mainly along the northern edge of Seram, and especially in the western part of SFTB (Teas et al., 2009).

Between the inner volcanic arc and outer arc lies the spectacular Weber deep that marks the deepest point (~7.2 km) of the Earth's oceans away from a trench. It is bounded by a major low angle (12°) normal fault system termed the Banda detachment in the east, which is exposed underwater over its 120 km down-dip and 450 km lateral extent with young extension at NW-SE direction (Pownall et al., 2016). Based on bathymetric analysis and plate reconstructions of Spakman and Hall (2010), Pownall et al. (2016) proposed that it was formed by forearc extension induced by southeastward subduction rollback since 2 Ma ago.

The SKSZ is the largest strike-slip fault in the Banda arc region, and has deformed most of the regional structural features, namely the outer arc, the Seram fold-thrust belt on upper plate, the Seram trough at the plate boundary, and possibly the Aru trough on the lower plate (Figure 1a). However, the origin of this fault system and its role in the regional geodynamics remain enigmatic, which we propose to investigate in this study.

4. Results

4.1. Structural Mapping on Bathymetry

The 25 m high-resolution bathymetry map used in this study covers most of the forearc of the Banda outer arc and a part of the Australian continental margin (Figure 2a). For the Seram island, the global ocean & land terrain models (GEBCO_2019) at 15 arc-second intervals is used to perform structural and seismicity analysis along the Kawa shear zone. Figure 2b shows a detailed structural map where the Seram trough is marked by the frontal thrust of the Seram fold-thrust belt whose overall trend changes from E-W north of Seram to NW-SE east of Seram, and turning to N-S south of the Kumawa region, following the curvature of the Banda arc (see also Adhitama et al., 2017). South and west of the trough lies the Seram fold-thrust belt that comprises a large number of closely spaced individual fault and fold structures. We mapped all these compressional structural fabrics with thin black lines to represent the overall structural pattern and deformational trend of the SFTB (Figure 2b). Note that the dip symbols of small faults are not indicated due to the unresolved hanging walls. Obviously, the Seram fold-thrust belt is dominated by compressional structures mostly parallel to the trough. A series of small strike-slip faults (i.e., thin blue lines) oblique or normal to the trough are also observed from 128.5° to 132° longitude and −3.5° to −2.5° latitude (Figure 2b), which seem to crosscut some folds and thrusts. These secondary structures are interpreted to result from the differential movement of folds and thrusts, which are similar to those observed in the Hikurangi accretionary prism (Davidson et al., 2020).

The most striking structure west of the Seram trough is the Kumawa fault, which generates a remarkable deformation zone on the seafloor and has caused a drastic change in the orientation of the frontal thrust from NNW to NWW at longitude 132°–133° (Figures 2a and 2b). Furthermore, the Kumawa fault shows variation in the sense of slip, that is, right-lateral slip in the northwest (131°–131.5°) and left-lateral slip in the southeast (131.5°–132.5°); a detailed interpretation is presented in Section 4.4.1. In addition to these upper plate structures, we have also mapped the N-S and NNE-SSW trending normal faults that mark the west bound for the Kumawa basin and Aru basin in the lower plate (Figure 2b). North of these normal faults lies the proposed Kumawa fault that has been covered by mass transport complexes (Adhitama et al., 2017; Hall et al., 2017). The nearly ~ E-W striking Terera-Aiduna strike-slip fault is located in the northmost of the Aru trough, which is interpreted as a young structure with a little or no displacement (Figure 2b; Hall et al., 2017).

We have also marked other major features identified by previous studies (e.g., Hall et al., 2017; Pownall et al., 2016), such as the Kawa shear zone, the Banda detachment and the associated groove structures on the exposed fault surface (Figure 2b). This detailed structural mapping provides an overview of regional tectonics. To characterize the strike-slip fault, three seismic profiles and three selected regions combined with earthquake data are used to image its subsurface structure and seafloor deformation.

4.2. Interpretation of Seismic Profiles

A 2D seismic profile across the Banda forearc, Seram fold-thrust belt, Seram trough, and the Australian continental margin is shown in Figure 3. The Kumawa fault lies within the Seram fold-thrust belt and is > 45 km from the Seram trough. The enlarged Figures 3b and 3c show the detailed structures of the Kumawa fault and the deformation front of the Seram fold-thrust belt. The Kumawa fault appears to mark the contact between two seismic sequences from SW to NE (Figure 3b). The most distinguished feature in the SW sequence is a package of seismic horizons with chaotic facies, moderate-strong amplitudes and some lateral continuity at 1.5–4 s depth in TWT, which is, however, not observed in the NE sequence. At depth, the Kumawa fault seems to extend all the way from above the basal detachment to the seafloor with an apparent 90° dip (Figure 3b). On the seafloor, its movement has created a small basin (1 km wide and 0.2 km deep) at 13 km distance (Figure 3b). The deformation front of the Seram fold-thrust belt is dominated by a series of imbricate thrust faults and associated folds whose growth have markedly deformed the seafloor to form distinct scarps (Figure 3b). These images clearly demonstrate that both the Kumawa fault and the frontal thrusts are active structures.

The seismic profile shown in Figure 4a crosses the same tectonic elements as that in Figure 3a, but shows a very distinct subsurface structure of the Kumawa fault ~30 km landward the Seram trough. The most distinguished feature on this profile is the abrupt termination of a bottom-simulation reflector (BSR) against

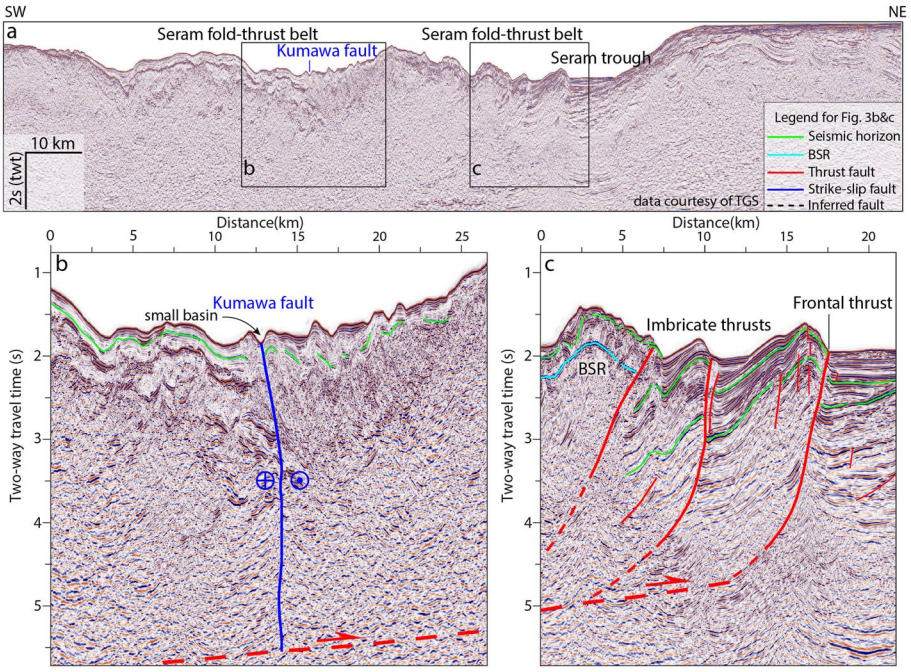


Figure 3. Structural interpretation on a seismic profile through the Seram region. For profile location see Figure 2. (a) Uninterpreted seismic profile with key structural features marked. (b) Interpreted seismic image showing the sub-surface structure of the northwest part of the Kumawa fault. Note the contrast in seismic facies on two sides of the fault. (c) Interpreted seismic image showing the deformation front of the Seram fold-thrust belt.

the Kumawa fault (at 25 km in Figure 4b). The BSR follows the seafloor reflection and represents a hydrate stability zone with gas hydrate saturated sediments above free gas filled sediments below (Singh et al., 1993). In addition to this, there are a few other sedimentary and structural features that allow us to constrain the Kumawa fault within the subsurface (Figure 4b), such as a zone of chaotic, moderate-high-amplitude seismic horizons at 1.5–3 s TWT depth landward of the Kumawa fault, and a series of imbricate thrust faults

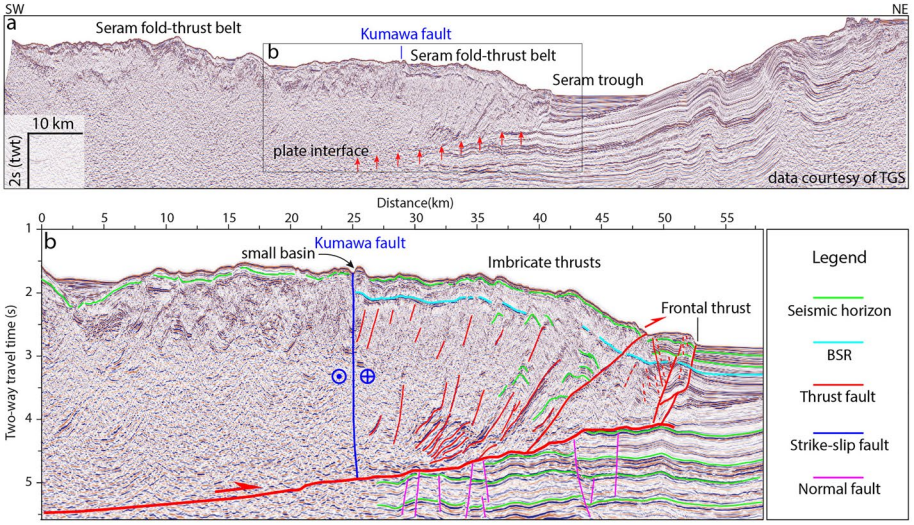


Figure 4. Structural interpretation on a seismic profile through the northeast Banda margin. For profile location see Figure 2. (a) Uninterpreted seismic image with key structural features indicated. (b) Interpreted seismic image showing the sub-surface structure of the middle part of the Kumawa fault. Note the abrupt termination of BSR against the Kumawa fault. (c) Interpreted seismic image showing the deformation front of the Seram fold-thrust belt. BSR stands for bottom simulation reflector.

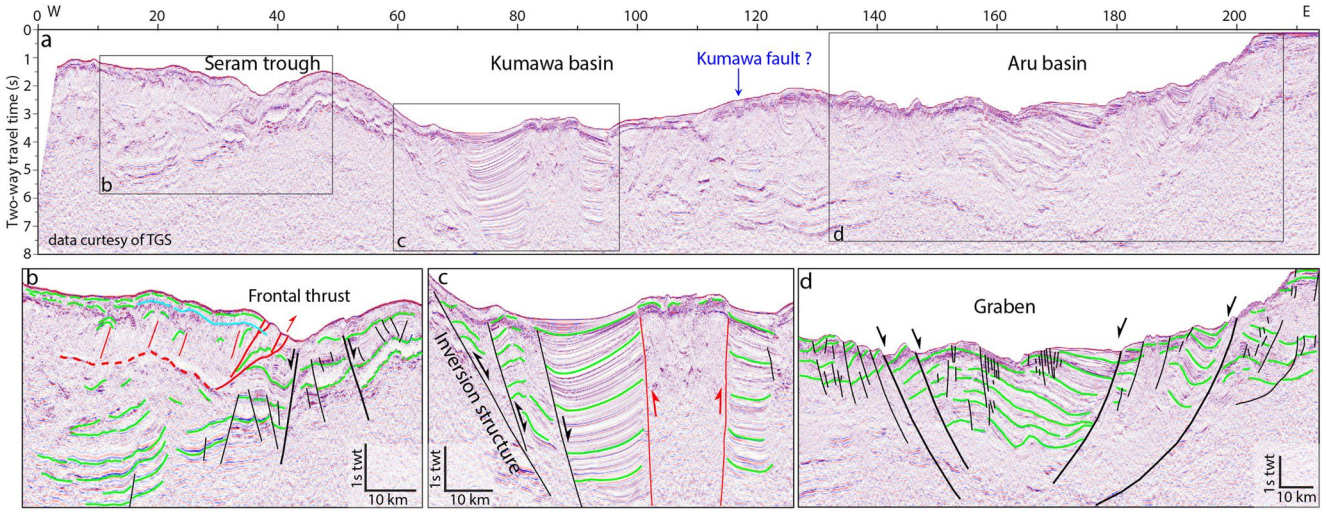


Figure 5. Structural interpretation on an E-W trending seismic profile across the Banda forearc, Seram trough and Aru trough. For profile location see Figure 2. (a) Uninterpreted seismic image with key structural domains indicated. (b) Interpreted seismic image across the Seram trough. (c) Interpreted seismic image showing the structures of the Kumawa basin, note the hanging wall anticlines related to tectonic inversion. (d) Interpreted seismic image showing the graben structure of the Aru basin.

trench-ward of the Kumawa fault. Similar to Figure 3a, the Kumawa fault extends from above the basal fault to the seafloor with a 90° dip and has formed a small basin of 1 km width and 0.2 km depth at its tip. The deformation front of the Seram fold-thrust belt is dominated by two major thrust faults that break the seafloor to form large abrupt scarps to the west. The rest of the imbricate thrusts appear to be buried without much seabed expression. Similarly, these observations suggest that the most active features in this seismic section are the two thrust faults at the front and the Kumawa fault (Figure 4).

Seismic profile shown in Figure 5a is oriented W-E and is a much longer profile compared to the above described two profiles, it extends from the Banda forearc on upper plate to the Aru trough on lower plate. We projected the location of the proposed Kumawa fault on this profile (at ~120 km in Figure 5a), but there does not seem to be any subsurface structures related to this fault. Additional evidence will be provided in Section 4.5 to resolve the presence/absence of the Kumawa fault in the Aru trough area. The Seram trough is rather narrow (Figure 5b), largely marking the convergent boundary between the strongly extended lower plate and the highly compressed overriding plate. The two frontal thrusts break the seafloor and together form a large scarp, suggesting they are active (Figure 5b). The rest of the thrust faults are poorly imaged, but seemingly blind without much seafloor expression. These are the early thrust faults possibly inactive due to back rotation, fault steepening and strain migration toward new frontal faults (Wu & McClay, 2011; Yang, Singh et al., 2020; Yang, Peel, et al., 2020).

The Kumawa basin lies on the hanging wall of a normal fault, which was later subjected to compression as tectonic inversion, forming a few minor anticlines on the hanging wall of the inverted fault (Figure 5c). These faults do not seem to be very active at present-day as they are overlain by a thick pile of growth sequence. Two high-angle conjugated thrust faults are observed in the basin with some seafloor expression, which are interpreted as a gravity-driven toe thrusts by Adhitama et al. (2017).

The Aru basin is deformed by a series of conjugated growth normal faults that together form a large graben (Figure 5d). Most of these normal faults are active as they all produce fault scarps on the seafloor. Four of these normal faults extended much deeper and formed relatively high scarps, and therefore, they are interpreted as basin-controlling faults.

Based on the above seismic interpretation (Figures 3–5), we can conclude that the most active structures in this region are the Kumawa fault, the deformation front of the Seram fold-thrust belt and the normal faults in the Aru basin, which we will discuss below.

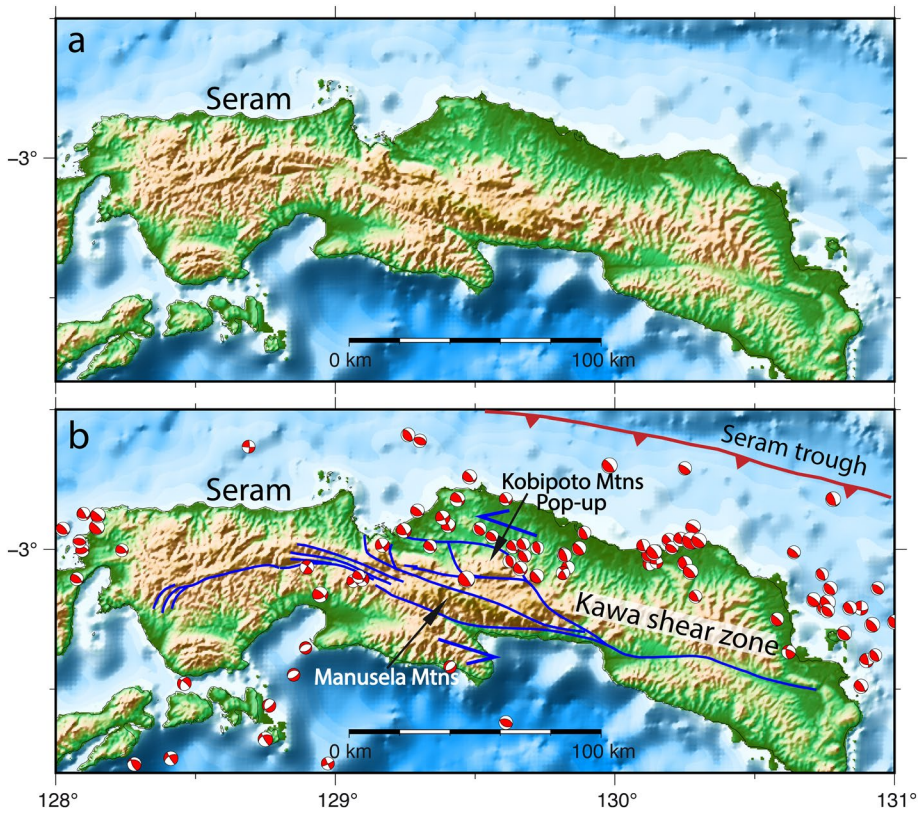


Figure 6. (a) Topography of the Seram island and (b) Topography map superimposed by the Kawa shear zone and seismicity. Topography and bathymetry are from Global ocean & land terrain models (https://www.gebco.net).

4.3. The Kawa Shear Zone on the Seram Island

The island of Seram has undergone considerable lithospheric extension throughout much of the Neogene (Pownall et al., 2013, 2014), which was attributed to its east-southeastward movement above the rolling-back Banda slab (Hall, 2012; Spakman & Hall, 2010). The Kawa shear zone on Seram (Figure 6) is a major lithospheric fault zone containing slivers of exhumed mantle and high-temperature metamorphic rocks (Pownall et al., 2013, 2017). The 40Ar/39Ar dating from mylonites adjacent to the Kawa shear zone recorded several episodes of thermal events from 3.4 Ma to 16 Ma (Pownall et al., 2017), possibly associated with several episodes of fault deformation. Based on the land topography and previous work, we mapped the WNW-ESE trending KSZ (Figure 6). We find that it is marked by a complex deformation zone comprising single fault strands in the east (130°–131°) and in the west (128°–129°) and a wide fault zone (~50 km width) in the center (129°–130°). While the single fault strands are associated with lateral displacement and extension, the central wide fault zone is characterized by shear zones, pop-up structures and uplifts (Pownall et al., 2013). Although the geomorphic features along the KSZ indicates a left-lateral sense of movement, the microstructural evidences suggest a complex history of both left and right lateral motions (Pownall et al., 2013). We plotted the seismicity on the Seram island and adjacent area, showing a few strike-slip events of both sinistral and dextral motions in the central portion of the KSZ (Figure 6) while the rest of the fault has no seismicity. Obviously, the KSZ presents structural and earthquake focal mechanism variations along strike with high fault activity and seismicity on its central complex deformation zone.

4.4. The Kumawa Fault

In the east of the Seram island, the bathymetry image clearly shows the ~120° striking, segmented Kumawa fault (Figure 7a). The seismicity data indicates a number of shallow thrust events on the Seram fold-thrust belt with only one earthquake at the SE extremity of the Kumawa fault (Figure 7a; see also Engdahl

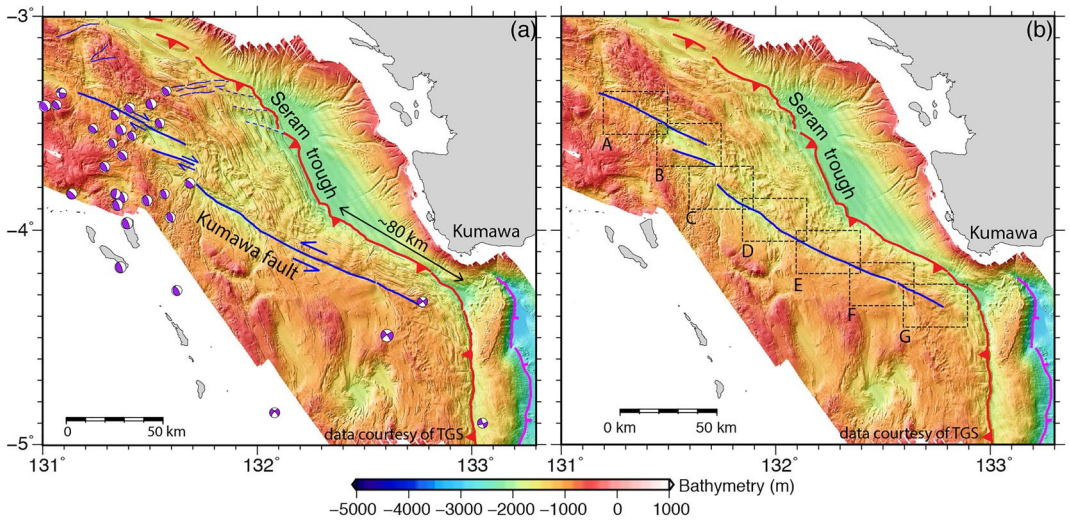


Figure 7. Mapping of the Kumawa fault on high-resolution bathymetry. (a) Mapped structures and earthquakes on bathymetry; note the 80 km displacement on the Seram trough caused by the Kumawa fault and a unique strike-slip earthquake at the SE extremity of the fault. (b) Bathymetry map showing the Kumawa fault, frontal thrust, location of selected regions A-G and bathymetry profiles for detailed structural and morphological analysis.

et al., 1998; McCaffrey, 1989). We have divided the fault into seven different areas from NW to SE to make detailed structural analysis, namely areas A to G. For instance, region B is dominated by a distinct pull-apart basin bounded by two parallel dextral strike-slip faults (Figure 7b). Southeastward of this basin, there is a slight southward shift of the fault from area B to C, indicating a right-lateral en echelon motion. The fault is sinistral from area C to G.

4.4.1. Structural Mapping

Among the seven selected areas, the areas A and G lies at the NW and SE extremities of the Kumawa fault, respectively (Figure 7b). In Figure 8, the area A shows sparse traces of fault, marked by blue arrows, probably representing a fault initiation (e.g., Kim & Sanderson, 2006). In contrast, area G exhibits clear, continuous fault trace, and distinct horsetail structures oblique to the main fault, similar to those observed at the extremity of other strike-slip faults (e.g., Granier, 1985; Gürboğa, 2016). These observations suggest that the Kumawa fault is likely to have initiated somewhere between these two extremities and then propagated laterally, rather than initiating at one extremity and propagating toward the other. Furthermore, the 2,000 Mw 5.2 strike-slip earthquake occurs on one of these secondary horsetail faults (Figure 8b) having NE-SW strike, consistent with the strike of the secondary horsetail fault. These observations will be important to decipher the tectonic history of the Kumawa fault. In contrast, the main Kumawa fault does not seem to have hosted any major earthquakes sine 1960s (Figure 7a), making its earthquake behavior intriguing. A detailed analysis of earthquake potential associated with the Kumawa fault is present at Section 5.3.

Horsetail structures at the extremity of strike-slip fault can be thrust faults, normal faults and strike-slip faults (Kim & Sanderson, 2006). Their specific styles are largely dependent on the local stress regime. Here, we made two topographic profiles (P1 and P2) normal to the horsetail structures (region G in Figure 8b), which combined with the focal mechanism of the 2000 earthquake, can help to decipher the fault types of these structures. Both topographic profiles clearly show a series of fault scarps that dip to southeast with variable vertical offsets ranging between 10 and 80 m (P1 and P2 in Figure 8c) at ~0.5–1.5 km apart. The focal mechanism of the 2000 earthquake indicates a NE-SW slip. Based on these details, we suggest that these structures are primarily strike-slip faults with dip-slip components. They are mainly formed on the northern side of the main fault whose sinistral slip results in local extensional stress fields, leading to the development of these horsetail faults (Region G in Figure 8b).

Area B is marked by a pull-apart basin with ~30 km length and ~15 km width (Figure 9a). The diamond shape of this basin implies a dextral slip along its two long edges. Two bathymetry profiles normal to the

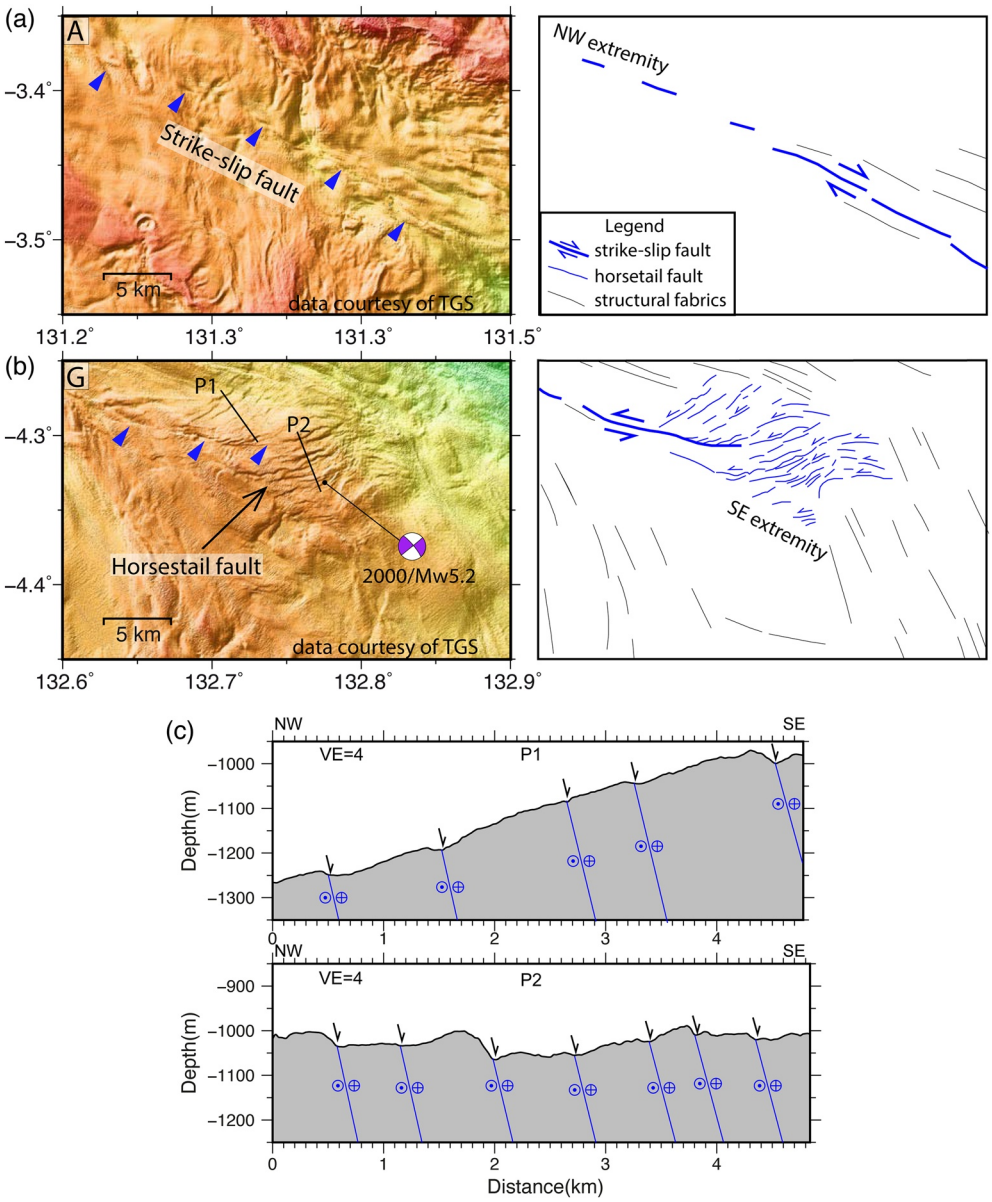


Figure 8. NW and SE extremities of the Kumawa fault. (a) The NW extremity of the fault expressed by sparse fault trace. (b) The SE extremity of the fault characterized by continuous fault trace and a number of horsetail structures oblique to the main fault. (c) Two dimensional bathymetry profiles across these features showing SE-dipping fault scarps. For location of area see Figure 7b.

faults highlight the morphology of the pull-apart basin and the distinct extensional deformation caused by the strike-slip faults and the associated normal faults (Figure 9a). Further southeastward, area C shows a 5-km-wide shear zone with no pull-apart basin, and seems to terminate against an NNE-trending valley-like feature at longitude 131.7° (Figure 9b). There is an obvious contrast between the regions B and C, both in the style of deformation and the sense of movement. Topographic profiles show an extensional basin and a SW dipping normal fault associated with the strike-slip faulting. Region D (Figure 9c) has a 5-km-wide zone of diffuse deformation, which seems to be bounded by a fault-parallel elongated basin on the SW side. The bathymetric profiles crossing this fault shows a topographic high bounded by two topographic lows, possibly a fault-controlled basin. We consider the structural styles of areas C and D to be similar.

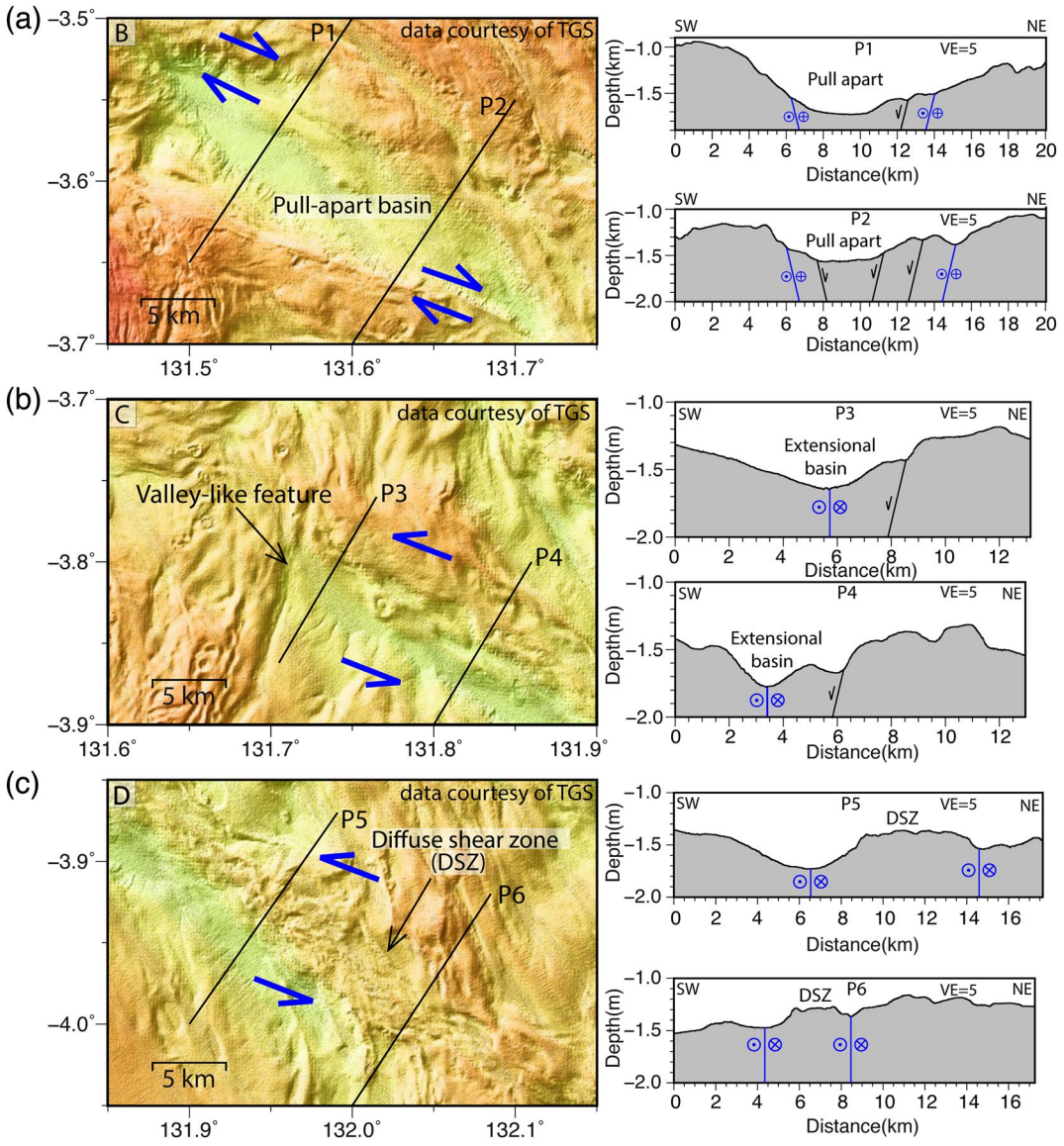


Figure 9. Fault analysis for area B, C, D along the Kumawa fault. (a) Pull-apart basin and related right-lateral slip (left), and 2D bathymetry profiles (right) across the basin. (b) Shear zone along the fault (left) and 2D bathymetry profiles (right) across it. (c) Diffuse shear zone along the fault (left) and 2D bathymetry profiles (right) through it. For location of area see Figure 7b.

Further southeastward lies the regions E and F (Figures 10a and 10b). Both regions show a clear, straight fault trace on the seafloor. There is no obvious diffuse shear zone along the fault as observed in areas C and D (Figures 9b and 9c). The topographic profiles validate this observation by showing a very narrow basin (<0.5 km width) at the fault tip (Figure 10), indicative of localized strain along the fault. Obviously, there is a distinct change in the structural style from areas C and D (Figure 9) to areas E and F (Figure 10). Area G is considered as the southeastward continuity of areas E and F as it also shows distinct fault trace on the bathymetry (Figure 10c).

4.4.2. Segmentation Along the Kumawa Fault

Based on the above structural analysis, three fault segments are identified along the Kumawa fault from NW to SE: (1) pull-apart basin; (2) diffuse shear zone; (3) distinct fault trace (Figure 11a). Eleven short topographic profiles through the segments 2 and 3 (Figure 11a) are used to measure the with and depth of

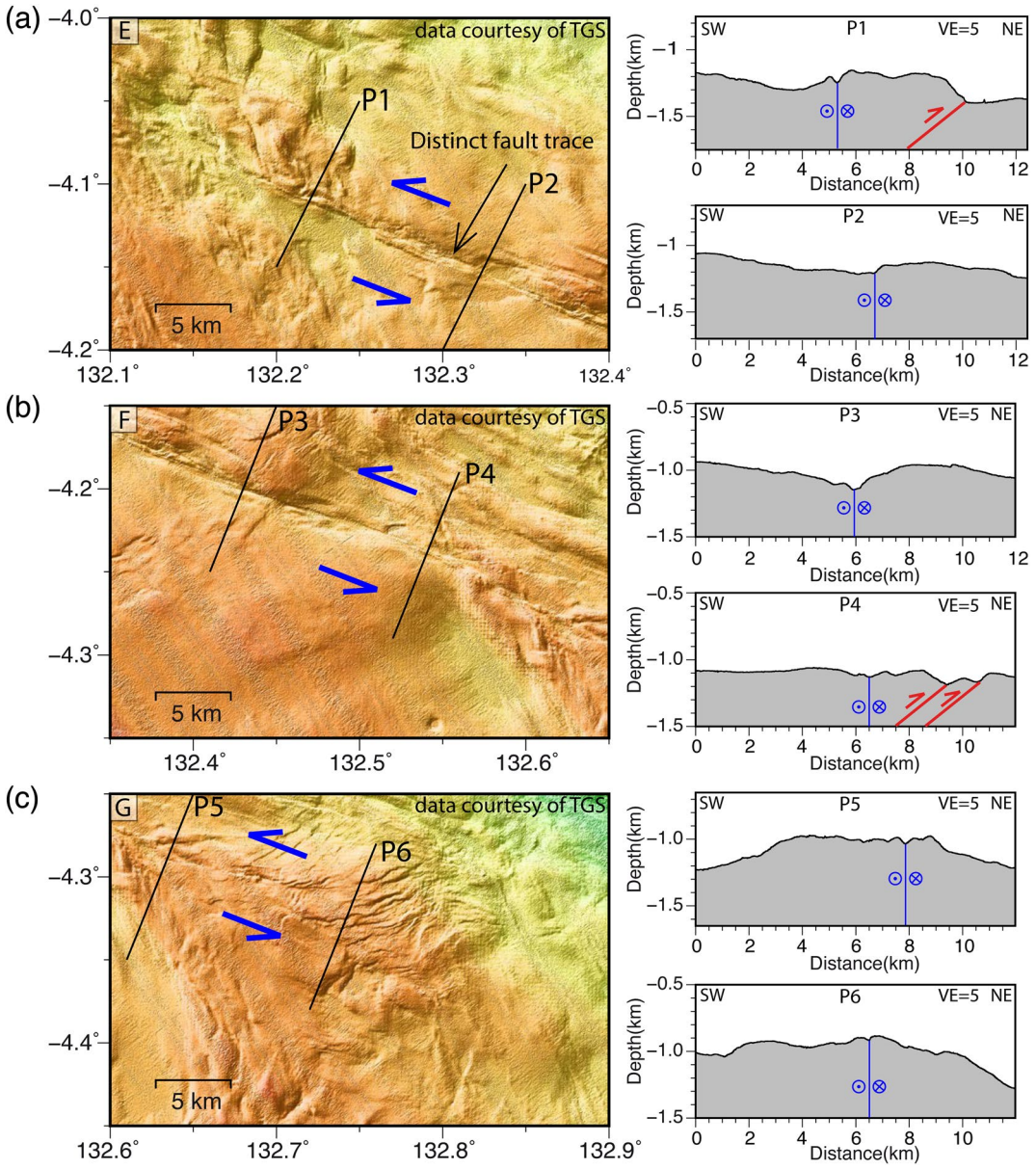


Figure 10. Fault analysis for area E,F,G along the Kumawa fault. (a) Distinct seafloor faulting (left) and 2D bathymetry profiles (right) across it. (b) Distinct fault trace on the seafloor (left) and 2D bathymetry profiles (right) across it. (c) Distinct seafloor faulting with oblique horsetail faults (left) and 2D bathymetry profiles across these features (right). For location of area see Figure 7b.

basin along the fault. As shown in Figures 11b and 11c, there is an overall decrease in both the basin width and the depth along the fault south-eastward, with the segment boundaries well marked by the changes in the basin widths and depths. These results also suggest that the Kumawa fault most likely initiated somewhere NW of the pull-apart basin in segment 1 and then propagated southeastward ending at the horsetail end of segment 3, similar to the direction of the subduction rollback (Spakman & Hall, 2010). The observed concave shape for the basin size in segment 2 (40–100 km in Figures 11b and 11c) suggests a local lateral fault growth/propagation.

To better visualize these fault segments, the 3D bathymetry models are established to align all the three segments together along the KF (Figure 12). Figure 12 shows that the pull-apart basin in the segment 1 lies within the topographic highs possibly related to compressional structures (see also Patria, 2016). The seg-

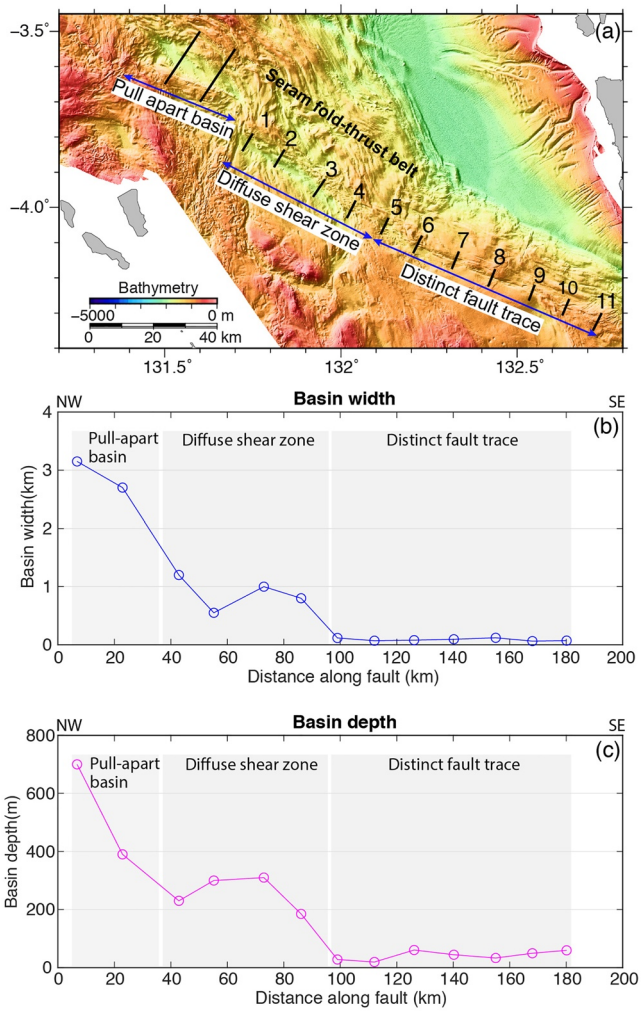


Figure 11. Segmentation of the Kumawa fault. (a) Classified three segments for the Kumawa fault from NW to SE: (1) Pull-apart basin, (2) Diffuse shear zone and (3) Distinct fault trace. Numbers 1–11 indicates the short bathymetry profile across the Kumawa fault. (b) Basin width along each segment. (c) Basin depth along each segment. Note a good correlation between the defined fault segments and the width and the depth of the basins. For the location of map see Figure 2a.

ment 2 is associated with elongated basin and adjacent diffuse shear zone whereas the segment 3 has a distinct fault trace on the seafloor parallel to the compressional structures.

4.5. Trough

The Kumawa basin and Aru basin are part of a narrow extensional system within the Aru trough on the northern Australian continental margin, located east of the U-shaped Banda Arc-Australia boundary (Figures 1, 2, and 13; Adhitama et al., 2017; Hall, 2017; Hall et al., 2017). The basin formation started during the Late Miocene and the basin underwent several periods of subsidence marked by multiple unconformities (Adhitama et al., 2017). A few normal faults are developed in response to the extension in this region: the N-S trending fault that bounds the Kumawa basin to the east and the NNE-SSW trending fault that marks the western boundary of the Aru basin (Figure 13a). The NNW trending thrust fault is the toe thrust of the mass transport complex (see also Adhitama et al., 2017). The E-W trending Tarera-Aiduna fault zone is a young structure with little displacement, marking the northern boundary of the Aru trough (Adhitama et al., 2017). A mass transport complex lying roughly between these major faults is deformed by a number of NNE-trending normal faults on the upslope and an NNW-tending thrust fault on the downslope (Figure 13a). Previous authors proposed that the Kumawa fault is buried beneath the mass transport complex (Figure 13a; Adhitama et al., 2017; Hall et al., 2017). To test this hypothesis, we plotted earthquakes in the region (Figure 13b), which exhibit a complex distribution of strike-slip and normal events. By integrating the structural map with focal mechanisms, we identify a possible network of strike-slip faults (black dashed lines in Figure 13b), rather than the single WNW-ESE-trending Kumawa fault proposed earlier (blue dashed line in Figure 13a). Further, the 3D bathymetry model does not show NW-SE trending bathymetric irregularities related to this Kumawa fault portion, such as displacement, shear zone, elongated minor basin or scarp (Figure 13c). By reconciling this evidence, we argue that the Kumawa fault does not exist in the Aru trough region. Instead, the Kumawa fault is confined to the forearc region of the Banda outer arc system, similar to strike-slip faults observed on other oblique subduction systems (e.g., Fitch, 1972; McCaffrey, 1992; Schütt & Whipp, 2020).

4.6. Seismicity in the East Banda Area

The seismicity map in the east Banda area (Figure 14a) highlights the absence of major seismicity in the Weber deep and along the Kumawa fault (see also Pownall et al., 2016; Špičák & Vaněk, 2013). Furthermore, there has been no great megathrust earthquake (M8+) along this collisional margin despite the 20 mm/yr convergence. Another important feature is the concentration of earthquakes in two regions, region A mainly with thrust events and region B hosting mainly normal events (see also Hall et al., 2017). Note that almost all the normal fault earthquakes in box B are actually distributed in the Aru basin, not in the Kumawa basin (Figures 13b and 14a). The thrust earthquake concentration (*A*) can be explained by the compressional deformation on the Seram fold-thrust belt (Engdahl et al., 1998; McCaffrey, 1989; Špičák & Vaněk, 2013) whereas the normal earthquakes are produced by the extensional deformation in the Aru basin (Figure 5; see also Adhitama et al., 2017).

Earthquake-depth profiles show possible source fault structures at depth (Figures 14b and 14c). Although there could be some uncertainties on the depths of these earthquakes, the vast majority of events along the strike in region A have depths ranging between 10 and 40 km, without any fault geometry. On the other

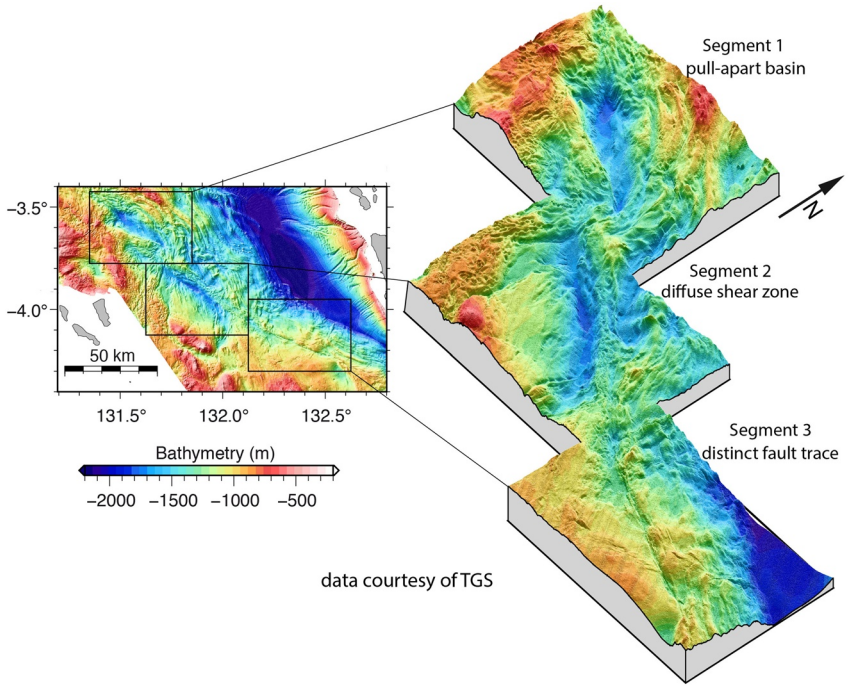


Figure 12. 3D bathymetry of the three segments of the Kumawa fault: pull-apart basin, diffuse shear zone and distinct fault trace. Note the legend for bathymetry in this figure is different from other figures. For the location of map see Figure 2a.

hand, the dip profile projected with distance from the trench (i.e., 0 km), shows wedge seismicity which dips to SW with an increasing angle from <10° (within 15 km away from trench) to 25° (>15 km away from trench), typical of thrust earthquake distribution in the upper plate of subduction zones (e.g., Liu & Zhao, 2018), possibly representing the plate interface, that is, megathrust (Figure 14b).

The along-strike earthquake profile from the region B also has the majority of earthquakes with depth ranging between 10 and 40 km (Figure 14c). However, a slight decrease in the earthquake population from NE to SW is observed, with slightly more seismicity between 0 and 80 km distance (Figure 14c). Similarly, the dip profile shows there are more events in the SE (between 40 and 80 km distance) and fewer events in NW (<40 km distance). From these observations it can be inferred that there is an earthquake concentration in the east and southeast of this region, indicative of strain migration toward E-SE in the Aru trough. This is compatible with the observed a number of normal faults in the Aru basin on the seismic profile (Figure 5).

5. Discussion

5.1. The Extent of the Seram-Kumawa Shear Zone

The spatial scale of an active strike-slip fault is important in estimating the length of co-seismic rupture and the possible magnitude of future large earthquakes (e.g., Clark & Cox, 1996; Wells & Coppersmith, 1994). Previous studies in the northern Banda arc region have mainly concentrated on the onshore portion of the Seram-Kumawa shear zone, that is, the Kawa shear zone, using petrological studies, geomorphological observations and geophysical surveys (Figure 1; e.g., Audley-Charles, 1975; Milsom, 2001; Pownall, 2015; Pownall et al., 2013, 2014, 2017; Tjokrosapoetro & Budhitrisna, 1982; Watkinson & Hall, 2017). It was not until 2016 that the Kumawa fault was first mapped using substantial multibeam bathymetry data (Figure 2a; Hall et al., 2017; Patria & Hall, 2017). Meanwhile, Adhitama et al. (2017) combined this data set with seismic profiles to study the basin history and petroleum system in the Aru trough, and proposed that a portion of the Kumawa fault is buried beneath the northern Aru trough. Hall et al. (2017) went on further to suggest that the Kawa shear zone, the Kumawa fault and the buried part, all are linked and form *a* >600 km long SKSZ from the west Seram island to the north Aru trough (Figure 1a).

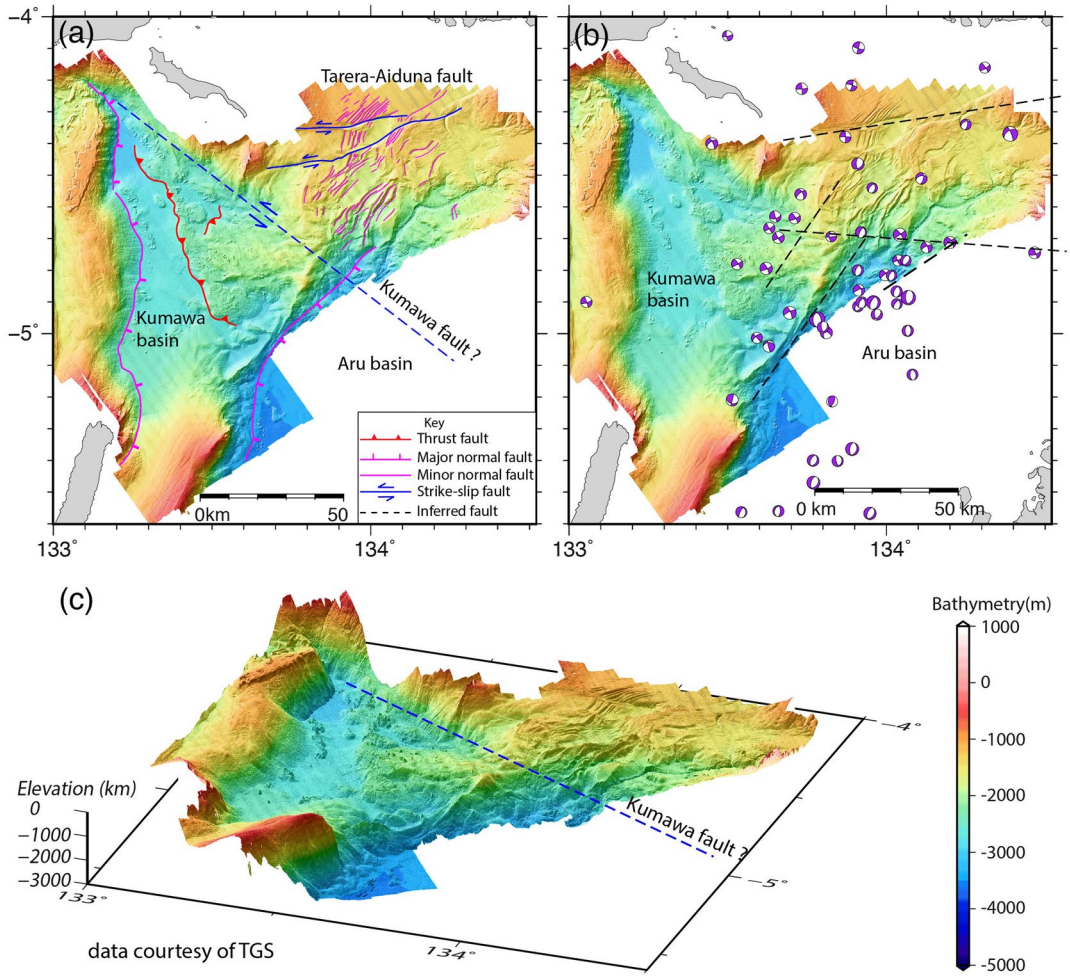


Figure 13. Structures and seismicity in the Aru trough. (a) The mapped fault structures and proposed blind Kumawa fault on bathymetry. (b) Bathymetry map along with earthquakes and approximated strike-slip faults (dash line) based on the earthquake distribution. (c) 3D bathymetry model of the Aru trough. There is no compelling evidence for the proposed Kumawa fault (Adhitama et al., 2017; Hall et al., 2017).

Based on several lines of evidences, here we argue that the Kumawa fault is absent in the Aru trough. First, given the proximity between the two parts of the Kumawa fault offshore SE Seram and in the Aru trough (~40 km apart, Figures 1a and 2), it is rather hard to explain their contrasting seafloor expressions, that is, a clear traces of seafloor faults SE Seram (Figures 2 and 7) but the absence of any seafloor fault trace in the Aru trough (Figure 13a). Second, the seismic images from the Aru trough does not show any subsurface fault structures at the proposed location of the KF by Adhitama et al. (2017) and Hall et al. (2017) (Figure 5a), which rules out the possibility that the KF is a proto strike-slip fault that is currently coalescing. Third, the seismicity in the Aru trough does not support the presence of a large, individual NW-SE trending KF, instead it shows a complicated strike-slip faults network (Figure 13b). Fourth, the strike-slip faults in oblique subduction zones are formed to varying extent by margin-parallel slip partitioning that are largely confined on the overriding plate (e.g., Fitch, 1972; McCaffrey, 1992; Schütt & Whipp, 2020). Therefore, we suggest that the Seram-Kumawa Shear Zone has two distinct segments (the Kawa shear zone and the Kumawa fault), and extends only up to west of the Seram trough on the overriding plate, similar to other strike-slip fault systems in oblique subduction zones (e.g., Calais et al., 1992; Ghosal et al., 2012; Laurencin et al., 2017; Manaker et al., 2008).

The Kawa shear zone and the Kumawa fault do not connect directly with each other at 131° (Figures 1 and 2). Instead, they are ~50 km apart with a slight N-S shift across the strike (at 131° in Figure 2b). The

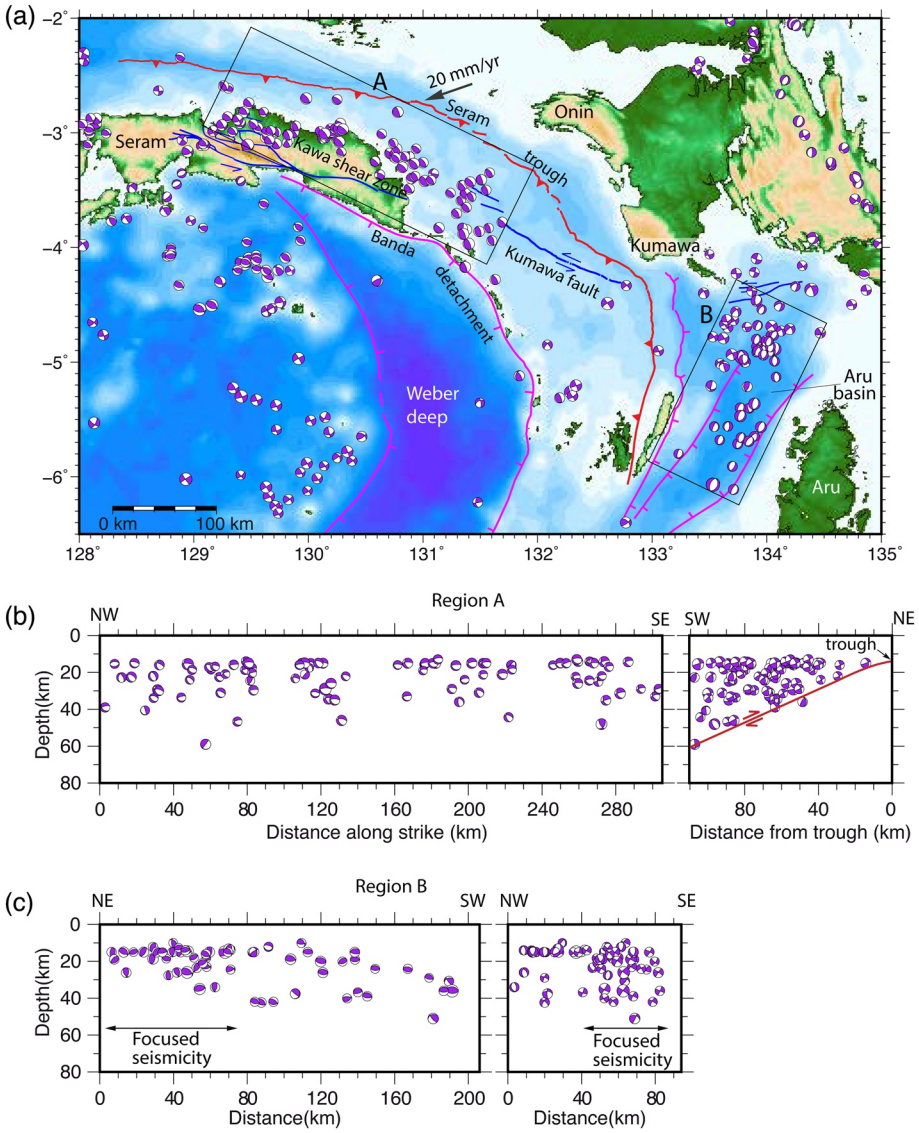


Figure 14. Seismicity on the east Banda margin. (a) Earthquakes and structural elements superimposed on bathymetry map. Note two earthquake concentration areas roughly at two sides of the Seram-Kumawa Shear Zone, and the absence of major seismicity in the Weber deep and along the Kumawa fault. (b) Earthquake 2D cross-sections along strike (left) and dip (right) in box A with focal mechanism projected laterally onto the sections, (c) Earthquake 2D cross-sections along strike (left) and dip (right) in box B with focal mechanism projected laterally onto the sections.

Kawa shear zone is a major lithospheric fault zone initiated at ~16 Ma with slivers of exhumed mantle peridotites (Pownall et al., 2013, 2014, 2017), and has a deformational zone up to 50 km wide at the central part marked by the Kobipoto mountains, pop-up structures and metamorphic core complex (Figure 6; Pownall et al., 2013, 2014) and hosted a few strike-slip earthquakes (Figure 6; Watkinson & Hall, 2017; this study). Offset geomorphic features, such as river streams and shutter ridges along this fault and the nearby Tehoru 1899 M7.8 tsunamigenic earthquake, all indicate that the Kawa shear zone has been active during Quaternary and is capable of generating large earthquakes (Brune et al., 2010; Watkinson & Hall, 2017). Furthermore, the Banda detachment has also been suggested to have caused destructive earthquakes, earthquake induced submarine landslides which in turn triggered large tsunamis (Cummins et al., 2020). In contrast, the Kumawa fault is a shallow crustal fault rooted at plate interface (Figures 3 and 4). It is linear and has a relatively narrow (<5 km) deformation zone (Figure 7), and there are no recent large earthquakes along this fault (Figure 7a). Regarding the timing, the Kumawa fault displaced the Seram fold-thrust belt of

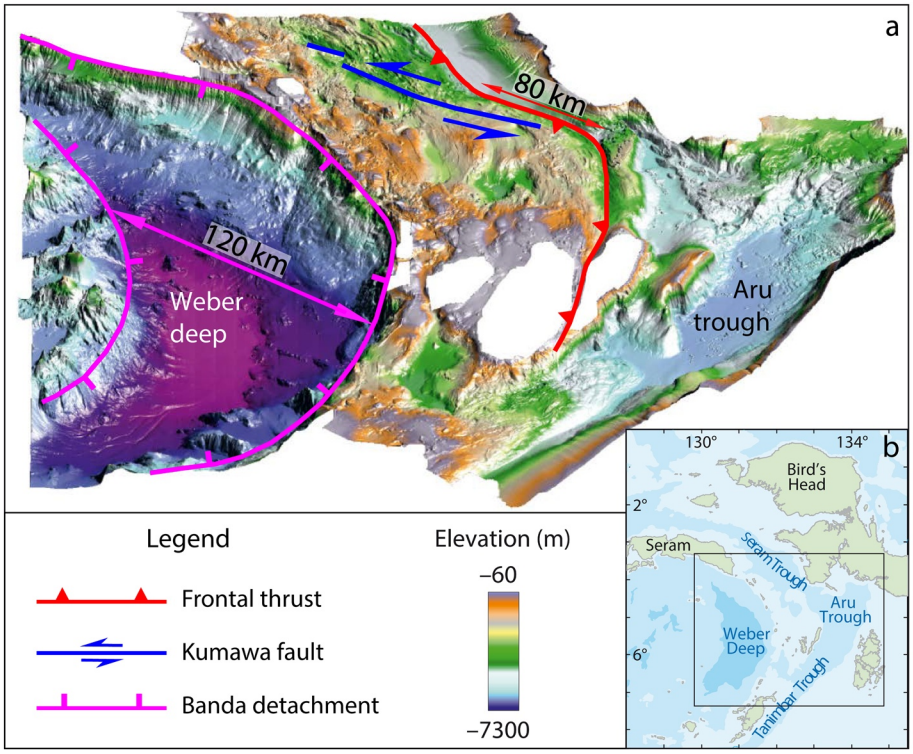


Figure 15. (a) 3D bathymetry map of the east Banda arc showing many similarities between the Banda detachment and the Kumawa falt, indicating their genetic links in tectonic origin; (b) regional map showing the location of Figure 15a, modified from Hall (2017).

<3.6 Ma age (Pairault et al., 2003), so it must be younger than 3.6 Ma. Based upon these lines of evidences, we interpret these two faults as two segments of the SKSZ that propagated southeastward from 16 Ma to <3.6 Ma.

5.2. The Tectonic Origin of the Kumawa Fault

Subduction rollback induces extension on the upper plate to fill the space created by the retreating trench (e.g., Carlson & Melia, 1984; Hall, 2017; Jolivet & Brun, 2010; Molnar & Atwater, 1978; van Hinsbergen et al., 2014). In east Indonesia, the southeastward Banda slab rollback is well documented by the opening up of the North Banda Sea between 12 and 7 Ma and the South Banda Sea between 6 and 2 Ma, and multiple extensions on the Seram island (Hall, 2017; Pownall et al., 2013, 2014, 2017). The 7.2-km Weber deep bounded by the Banda detachment in the east is the product of the last stage of extension since 2 Ma ago (Pownall et al., 2016).

Although the Kumawa fault and the Banda detachment are different structures in terms of fault type and fault angle, that is, high-angle strike-slip fault versus low angle normal fault, they have many features in common, implying a possible genetic link. Specifically, both faults show a similar strike, that is, WNW-ESE (Pownall et al., 2016, Figures 2b and 15). Regarding the timing, the Banda detachment is 2 Ma old and formed at the last stage of subduction rollback (Hall, 2012; Pownall et al., 2016). The Kumawa fault is younger than 3.6 Ma as it partially offsets the SFTB of <3.6 Ma old (Pairault et al., 2003, Figure 7). The amounts of deformation on these two structures are of similar scale (Figure 16), that is, 120 km extension on the Banda detachment (Pownall et al., 2016) and 80 km displacement on the Kumawa fault (Hall et al., 2017; this study). Previous studies proposed that the Banda detachment propagated southeastward, the same direction as the subduction rollback (Pownall et al., 2016). The observed horsetail structures at the Kumawa fault's SE extremity (Figure 8b) and southeastward decreasing basin widths and depths along the fault (Figures 11 and 12) indicate a southeastward fault propagation. The prominent seafloor faulting (Fig-

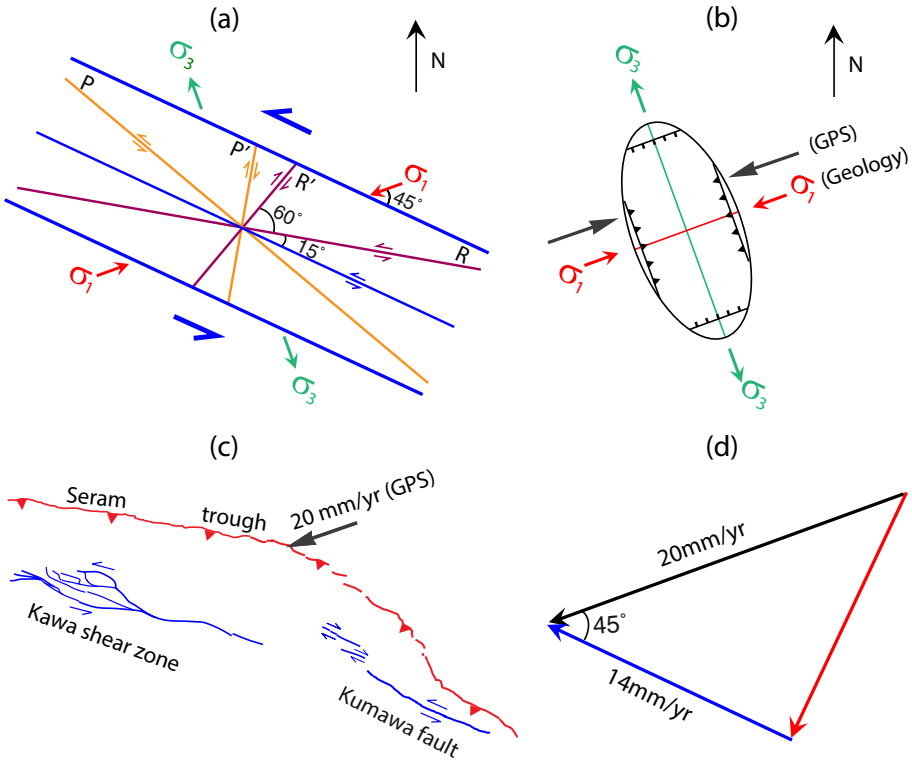


Figure 16. Slip rate of the Seram-Kumawa Shear Zone and maximum stress orientation across the northeast Banda margin. (a) Predicted maximum stress orientation from the Riedel Shear Model. (b) Maximum stress orientation determined by GPS measurement. Maximum stress orientations estimated from two methods are in good agreement. (c) Regional structures and rate of plate convergence. (d) Estimated slip rate along the SKSZ according to the triangular relationship between different slip vectors. σ_1 and σ_3 are principal stress axes, R synthetic Riedel shear, R′ antithetic Riedel shear, P secdonary synthetic shear, P′ secdonary antithetic shear.

ure 15), and the absence of major seismicity (Figure 14a) on these two structures suggest they have similar fault behavior. Lastly, they are probably crustal structures, that is, the 7.2 km depth below sea level for the Banda detachment (Figure 15) and the Kumawa fault being limited to the upper plate (Figures 3 and 4). These similarities between the Kumawa fault and the Banda detachment suggest that are likely coupled as the same large tectonic system in association with the rollback of the Banda slab during the last 2 Ma.

Pownall et al. (2016) noted that the Kawa shear zone that may have effectively become the northern termination of the Banda detachment. As discussed above (Section 5.1), both the KSZ and KF belongs to the same large fault system of SKSZ but formed at different times, the KSZ formed during the 2–16 Ma subduction rollback as documented by the multiple extension and thermal events along this shear zone (Hall, 2017; Pownall et al., 2013, 2014, 2017), while the KF is a product of the last 2 Ma subduction rollback. Tectonically, they are the similar responses of overriding plate extension induced by subduction rollback but at different stages.

Another possible contribution to the evolution of the Kumawa fault is the oblique arc-continent collision. Riedel shear model predicts a ~45° angle between the maximum stress orientation and the strike-slip orientation. Based on this principle, we rotated the model to make its shear orientation parallel to the Kumawa fault and the Kawa shear zone, which predicts a WSW-ENE maximum stress orientation (σ_1) across the Banda margin (Figure 16a). This orientation is largely consistent with the current plate convergence orientation determined by GPS measurements (Figure 16b; Bock et al., 2003; Simons et al., 2007), indicating possible contribution of oblique collision to the formation of the KF. Although the KF initiated 2 Ma ago and the GPS measurement only represents the present plate convergence, this consistency is important, and therefore the role of the arc-continent collision in the evolution of the KF should be important since it is synchronous with the last 2 Ma slab rollback and is close to the KF (Hall et al., 2017; Pownall et al., 2016; Spakman

& Hall, 2010). Furthermore, this comparison also allows us to approximate the current rate of slip along the KF. If the slip vector of 20 mm/yr arc-continent collision (Bock et al., 2003; Simons et al., 2007) is fully partitioned into the margin-normal thrusting along the Seram trough and the margin-oblique transcurrent motion along the Kawa shear zone and the Kumawa fault, that is, SKSZ (Figure 16c), the established simple right triangle relation between these slip vectors (Figure 16d) yields a slip rate of 14 mm/yr along the SKSZ. This should be the maximum value because there might be other deformations taking up partitioned slip, such as layer parallel strain (Koyi et al., 2004), lateral compaction (Butler & Paton, 2010), and slip across the Seram fold-thrust belt (Pairault et al., 2003; Patria & Hall, 2017; Sapin et al., 2009).

Since subduction rollback is the most important geodynamic process in the east Banda region in the Neogene time (e.g., Hall, 2017; Hall & Spakman, 2015; Spakman & Hall, 2010), it must have played a dominant role in the Banda arc deformation for the last ~16 Ma, while the oblique collision is only one consequence of this process (Spakman & Hall, 2010) and has relatively much less control on the upper plate extension. Therefore, we propose that the Kumawa fault is formed mainly by the upper plate extension induced by the subduction rollback during the last 2 Ma, with minor contribution from the oblique collision. Its estimated geological slip rate is 40 mm/yr, with an offset of 80 km over 2 Ma.

5.3. Seismicity Along the Kumawa Fault

As an important regional structure marked by 80 km displacement and distinct seafloor faulting, the Kumawa fault mysteriously lacks major seismicity (Figures 7a and 14a), similar to the Banda detachment (Figure 14a; Pownall et al., 2016; Špičák & Vaněk, 2013). Three ideas have been invoked to explain the absent seismicity on the Banda detachment: (1) fault inactivity, (2) fault locking and (3) aseismic slip. As the two structures seems to be coupled in the same geodynamic process (Section 5.2), these ideas can also apply to the Kumawa fault. There is no strong evidence to suggest that the Banda subduction rollback is fully terminated (Pownall et al., 2016; Spakman & Hall, 2010), and given the proximity between the KF and the Seram trough across which a 20 mm/yr collision (Bock et al., 2003; Simons et al., 2007) is occurring, the KF is unlikely to be inactive. In addition, the fault trace on the seafloor also attest that Kumawa fault is a tectonically active feature. Instead, it is possible that a slip component of this oblique collision is partitioned into the Kumawa fault, that is, <14 mm/yr slip rate (Figure 16d), but this value is only 17.5% of the 40 mm/yr geological slip rate of the Kumawa fault, that is, substantial reduction. The slip along the strike slip fault could operate through aseismic creep (e.g., Çakir et al., 2012), related to pervasive deformation, reduced fault friction and microseismicity. However, it is difficult to test this scenario without this information. Instead, the segment of distinct fault trace on the KF is suggestive of localized deformation (Figures 11 and 12), rather than pervasive deformation. The occurrence of a Mw 5.2 earthquake on the horsetail fault of KF (Figure 8b) indicates a certain level of earthquake-related activity associated with the main fault. As such, we are in favor of the second hypothesis that the fault is partially locked, with a lower slip rate of <14 mm/yr.

As *a* <20-km-long secondary fault can generate a Mw 5.2 earthquake (Figure 8a), if the more than 200-km-long, currently locked Kumawa fault was to completely rupture during a future large earthquake, the damage would be catastrophic. Further study is required to develop a fine 3D model for this fault, estimate the area of fault plane, determine the temporal slip, the state of stress, and assess the maximum earthquake potential.

5.4. Comparison With Other Margin-Oblique Strike-Slip Faults

Similar to the Kumawa fault, margin-oblique strike-slip faults cross the deformation front of accretionary wedge are also observed elsewhere, such as Cascadia (Goldfinger et al., 1997), Barbados Ridge (Caribbean Sea, DiLeonardo et al., 2002), and the Hikurangi subduction zone (Davidson et al., 2020). However, all these faults are spatially near the subduction front (not extending to the inner forearc and rear of accretionary prism), short in length (several tens of kilometers), of little displacement (several kilometers). The conjugated strike-slip faults at Hikurangi margin just straddle a subducting seamount, and are ephemeral and overprinted by the formation of new structures as the seamount subduction advances (Davidson et al., 2020). Therefore, these structures are unlikely to have great impact on the geodynamic process of subduction zones.

The Kumawa fault has been formed since ~2 Ma ago (Figures 1 and 2), and does not seem to be an ephemeral feature. It extends >200 km across the Banda forearc (Figure 7) and cross-cuts the entire overriding plate (Figures 3 and 4) with strong seafloor faulting (Hall et al., 2017; Patria et al., 2017; this study), that is, not a small structure. Seismicity map shows that there are no large earthquakes (Magnitude >8) in the east Banda margin (Figure 14a) despite a 20 mm/yr plate convergence. Along the KF there are much more thrust earthquakes on its north-northeast side than its south-southeast side (Figure 14a; see also Špičák and Vaněk, 2013). The abrupt strike change and the 80-km displacement of the deformation front caused by the KF indicates that the continuity of the megathrust fault is affected by this fault (Figure 7). The 14–40 mm/yr slip rate of KF should have accommodated a considerable amount of slip derived from the oblique plate convergence (Figures 1b and 16d), leaving less margin-normal slip on the megathrust and other structures. The paleo-trench has been overridden by the continued upper-plate collision, and therefore the typical ocean-continent collisional boundary is no longer preserved (e.g., Pairault et al., 2003). Furthermore, the Kumawa fault perhaps has limited the extent of the frontal thrust that could be locked. Therefore, a large magnitude earthquake is unlikely in this setting.

Subduction rollback is a common plate tectonic process. Not only does it cause trench to retreat, but also can displace the trench and limit the lateral extent of megathrust thrust earthquakes due to the presence of large-scale margin-oblique strike-slip faulting on the upper plate. This study calls for more attention on such a complex and important tectonic process and its role on the overriding plate deformation and great earthquake potential on plate interface.

6. Conclusion

The WNW-ESE-trending Seram-Kumawa Shear Zone is an important regional structure in the Banda forearc region in east Indonesia. Here we have combined multibeam bathymetry, marine seismic reflection data with earthquake data to study the geometry, structure, deformation, and driving mechanism of this remarkable fault and its hazard potential. Our new results draw the following conclusions:

(1) The Seram-Kumawa Shear Zone is composed of two segments: a ~200-km-long Kawa shear zone on the Seram island and another ~200-km-long-Kumawa fault offshore SW Seram. Both are confined to the upper plate
(2) The Kawa shear zone is a lithospheric structure with a slight curvature, has a 50-km wide complex deformational zone with the earthquake concentration in the central part and only a few hundred meters of displacement during Quaternary, while the Kumawa fault is a straight, crustal fault with the depth rooted on the plate interface, has a ~ 80 km displacement in the last 2 Ma, and shows absence of seismicity
(3) Both the Kumawa fault and the Banda detachment share many similar features, that is, 120°–130° strike, shallow depth, distinct seafloor faulting, deformation scale (80–120 km), lack of seismicity, southeastward propagation, timing of evolution (~2 Ma), indicating their genetic connections. The Kumawa fault is interpreted to primarily result from the upper plate extension induced by the subduction rollback, with only a limited contribution from the oblique Banda arc-continent collision
(4) The Kumawa fault comprises three segments from NW to SE: pull-apart basin, diffuse shear zone and distinct fault trace, possibly due to the episodic extension on the upper plate within the last 2 Ma
(5) The Kumawa fault is presently slipping at a rate of <14 mm/yr, that is 17.5% of its 40 mm/yr geological slip rate. This significant reduction, together with the remarkable seafloor fault expression, the 80-km displacement and an Mw 5.2 earthquake on its secondary horsetail fault, suggests that the Kumawa fault is partially locked at present and awaiting a large event in the future
(6) The Kumawa fault has cut through the entire upper plate, displaced the frontal thrust and limited the extent of megathrust fault, making the occurrence of great earthquake along the east Banda margin unlikely. Such similar structural, tectonic and geohazard effect may be also applicable to other settings that experience subduction rollback and induced upper plate extension

Data Availability Statement

The high-resolution bathymetry image and marine seismic profiles used in this study are available from https://doi.org/10.6084/m9.figshare.14169581.

Acknowledgment
The authors thank Jonathan Pownall and an anonymous reviewer for their robust reviews and constructive comments that significantly improved the paper. The authors thank editor Jonathan Aitchison and Derya Gürer for handling of this paper with prompt action and providing helpful suggestions. The multibeam bathymetry and seismic reflection data for this study were provided by TGS for scientific research. The study leading to these results has received funding from the European Research Council under the European Union's Seventh Framework Programme (FP7/2007–2013)/ERC Advance Grant agreement no 339442 TransAtlanticILAB. Most Figures presented in this study are plotted using Generic Map Tools (Wessel et al., 2019). This is IPGP contribution NO. 4208.

References

Abbott, M., & Chamalaun, F. (1981). Geochronology of some Banda Arc volcanics. In A. J. Barber, & Wiryosujono (Eds.), The geology and tectonics of eastern Indonesia (Vol. 2) (pp. 253–268). Indonesia: Geological Research and Development Centre Special Publication.

Adhitama, R., Hall, R., & White, L. T. (2017). Extension in The Kumawa Block, West Papua, Indonesia. *Proceedings, 41st Annual Convention Indonesian Petroleum Association*. *2017*, 1–17. https://doi.org/10.29118/IPA.50.17.125.G

Audley-Charles, M. (1975). The Sumba fracture: A major discontinuity between eastern and western Indonesia. *Tectonophysics*, *26*(3–4), 213–228. https://doi.org/10.1016/0040-1951(75)90091-8

Barberi, S., Bigioggero, B., Innocenti, F., Marinelli, G., & Slejko, D. (1987). The island of Sumbawa: A major structural discontinuity in the Indonesian arc. *Bollettino Della Societa Geologica Italiana*, *106*(4), 547–620.

Bock, Y., Prawirodirdjo, L., Genrich, J., Stevens, C., McCaffrey, R., Subarya, C., et al. (2003). Crustal motion in Indonesia from global positioning system measurements. *Journal of Geophysical Research*, *108*(B8), 2367. https://doi.org/10.1029/2001jb000324

Bowin, C., Purdy, G., Johnston, C., Shor, G., Lawver, L., Hartono, H., & Jezek, P. (1980). Arc-continent collision in Banda Sea region. *AAPG Bulletin*, *64*(6), 868–915. https://doi.org/10.1306/2F9193CD-16CE-11D7-8645000102C1865D

Brune, S., Babeyko, A. Y., Ladage, S., & Sobolev, S. V. (2010). Landslide tsunami hazard in the Indonesian Sunda Arc. *Natural Hazards and Earth System Sciences*, *10*(3), 589–604. https://doi.org/10.5194/nhess-10-589-2010

Butler, R. W. H., & Paton, D. A. (2010). Evaluating lateral compaction in deepwater fold and thrust belts: How much are we missing from "nature's sandbox". *Geological Society of America*, *20*(3), 4–10. https://doi.org/10.1130/gsatg77a.1

Çakir, Z., Ergintav, S., Özener, H., Dogan, U., Akoglu, A. M., Meghraoui, M., & Reilinger, R. (2012). Onset of aseismic creep on major strike-slip faults. *Geology*, *40*(12), 1115–1118. https://doi.org/10.1130/g33522.1

Calais, E., Béthoux, N., & de Lépinay, B. M. (1992). From transcurrent faulting to frontal subduction: A seismotectonic study of the northern Caribbean plate boundary from Cuba to Puerto Rico. *Tectonics*, *11*(1), 114–123. https://doi.org/10.1029/91tc02364

Calais, E., Freed, A., Mattioli, G., Amelung, F., Jónsson, S., Jansma, P., et al. (2010). Transpressional rupture of an unmapped fault during the 2010 Haiti earthquake. *Nature Geoscience*, *3*(11), 794–799. https://doi.org/10.1038/ngeo992

Cardwell, R. K., & Isacks, B. L. (1978). Geometry of the subducted lithosphere beneath the Banda Sea in eastern Indonesia from seismicity and fault plane solutions. *Journal of Geophysical Research*, *83*(B6), 2825–2838. https://doi.org/10.1029/jb083ib06p02825

Carlson, R. L., & Melia, P. J. (1984). Subduction hinge migration, *Tectonophysics*,*102*, 399–411. https://doi.org/10.1016/0040-1951(84)90024-6

Charlton, T. R. (2010). The Pliocene-Recent Anticlockwise Rotation of the Bird's Head, the Opening of the Aru Trough–Cendrawasih Bay Sphenochasm, and the Closure of the Banda Double Arc. *Proceedings, 34th Annual Convention Indonesian Petroleum Association*, *156*, 265–287. https://doi.org/10.1016/j.jseaes.2018.02.004

Clark, R., & Cox, S. (1996). A modern regression approach to determining fault displacement-length scaling relationships. *Journal of Structural Geology*, *18*(2–3), 147–152. https://doi.org/10.1016/s0191-8141(96)80040-x

Cummins, P. R., Pranantyo, I. R., Pownall, J. M., Griffin, J. D., Meilano, I., & Zhao, S. (2020). Earthquakes and tsunamis caused by low-angle normal faulting in the Banda Sea, Indonesia. *Nature Geoscience*, *13*, 312–318. https://doi.org/10.1038/s41561-020-0545-x

Das, S. (2004). Seismicity gaps and the shape of the seismic zone in the Banda Sea region from relocated hypocenters. *Journal of Geophysical Research*, *109*(B12). https://doi.org/10.1029/2004jb003192

Davidson, S. R., Barnes, P. M., Pettinga, J. R., Nicol, A., Mountjoy, J. J., & Henrys, S. A. (2020). Conjugate strike-slip faulting across a subduction front driven by incipient seamount subduction. *Geology*, *48*(5), 493–498. https://doi.org/10.1130/g47154.1

DeMets, C., Gordon, R. G., Argus, D. F., & Stein, S. (1994). Effect of recent revisions to the geomagnetic reversal time scale on estimates of current plate motions. *Geophysical Research Letters*, *21*(20), 2191–2194. https://doi.org/10.1029/94gl02118

DiLeonardo, C. G., Moore, J. C., Nissen, S., & Bangs, N. (2002). Control of internal structure and fluid-migration pathways within the Barbados Ridge décollement zone by strike-slip faulting: Evidence from coherence and three-dimensional seismic amplitude imaging. *Geological Society of America Bulletin*, *114*(1), 51–63. https://doi.org/10.1130/0016-7606(2002)114<0051:coisaf>2.0.co;2

Engdahl, E. R., van der Hilst, R., & Buland, R. (1998). Global teleseismic earthquake relocation with improved travel times and procedures for depth determination. *Bulletin of the Seismological Society of America*, *88*(3), 722–743.

Fitch, T. J. (1972). Plate convergence, transcurrent faults, and internal deformation adjacent to southeast Asia and the western Pacific. *Journal of Geophysical Research*, *77*(23), 4432–4460. https://doi.org/10.1029/jb077i023p04432

Gürboğa, Ş. (2016). The termination of the North anatolian fault system (NAFS) in Eastern Turkey. *International Geology Review*, *58*(12), 1557–1567. https://doi.org/10.1080/00206814.2016.1175976

Ghosal, D., Singh, S., Chauhan, A., & Hananto, N. (2012). New insights on the offshore extension of the Great Sumatran fault, NW Sumatra, from marine geophysical studies. *Geochemistry, Geophysics, Geosystems*, *13*(11). https://doi.org/10.1029/2012gc004122

Goldfinger, C., Kulm, L. D., Yeats, R. S., McNeill, L., & Hummon, C. (1997). Oblique strike-slip faulting of the central Cascadia submarine forearc. *Journal of Geophysical Research*, *102*(B4), 8217–8243. https://doi.org/10.1029/96jb02655

Granier, T. (1985). Origin, damping, and pattern of development of faults in granite. *Tectonics*, *4*(7), 721–737. https://doi.org/10.1029/tc004i007p00721

Hall, R. (1996) Reconstructing Cenozoic SE Asia. *Geological Society, London, Special Publications*, *106*, 153–184. https://doi.org/10.1144/gsl.sp.1996.106.01.11

Hall, R. (2002). Cenozoic geological and plate tectonic evolution of SE Asia and the SW Pacific: computer-based reconstructions, model and animations. *Journal of Asian Earth Sciences*, *20*(4), 353–431. https://doi.org/10.1016/s1367-9120(01)00069-4

Hall, R. (2012). Late Jurassic-Cenozoic reconstructions of the Indonesian region and the Indian Ocean. *Tectonophysics*, *570–571*, 1–41. https://doi.org/10.1016/j.tecto.2012.04.021

Hall, R. (2017). Southeast Asia: New views of the geology of the Malay Archipelago. *Annual Review of Earth and Planetary Sciences*, *45*, 331–358. https://doi.org/10.1146/annurev-earth-063016-020633

Hall, R., Patria, A., Adhitama, R., Pownall, J. M., & White, L. T. (2017). Seram, the Seram Trough, the Aru Trough, the Tanimbar Trough and the Weber Deep: A new look at major structures in the eastern Banda Arc. *Proceedings, 41st Annual Convention Indonesian Petroleum Association*, *41*, IPA17-91. https://doi.org/10.29118/IPA.50.17.91.G

Hall, R., & Spakman, W. (2015). Mantle structure and tectonic history of SE Asia. *Tectonophysics*, *658*, 14–45. https://doi.org/10.1016/j.tecto.2015.07.003

Hamilton, W. B. (1979). Tectonics of the Indonesian Region (Vol. 1078). US Government Printing Office. Retrieved from https://www.worldcat.org/title/tectonics-of-the-indonesian-region/oclc/3706013

Harris, R. A. (1992). Peri-collisional extension and the formation of Oman-type ophiolites in the Banda Arc and Brooks Range. *Geological Society, London, Special Publications*, *60*(1), 301–325. https://doi.org/10.1144/gsl.sp.1992.060.01.19

Hinschberger, F., Malod, J.-A., Dyment, J., Honthaas, C., Réhault, J.-P., & Burhanuddin, S. (2001). Magnetic lineations constraints for the back-arc opening of the Late Neogene South Banda Basin (eastern Indonesia). *Tectonophysics*, *333*(1–2), 47–59. https://doi.org/10.1016/s0040-1951(00)00266-3

Hinschberger, F., Malod, J. A., Réhault, J. P., & Burhanuddin, S. (2003). Contribution of bathymetry and geomorphology to the geodynamics of the East Indonesian Seas. *Bulletin de la Societe Geologique de France*, *174*(6), 545–560. https://doi.org/10.2113/174.6.545

Hinschberger, F., Malod, J.-A., Réhault, J.-P., Villeneuve, M., Royer, J.-Y., & Burhanuddin, S. (2005). Late Cenozoic geodynamic evolution of eastern Indonesia. *Tectonophysics*, *404*(1–2), 91–118. https://doi.org/10.1016/j.tecto.2005.05.005

Honthaas, C., Réhault, J.-P., Maury, R. C., Bellon, H., Hémond, C., Malod, J.-A., et al. (1998). A Neogene back-arc origin for the Banda Sea basins: Geochemical and geochronological constraints from the Banda ridges (East Indonesia). *Tectonophysics*, *298*(4), 297–317. https://doi.org/10.1016/s0040-1951(98)00190-5

Jolivet, L., & Brun, J.-P. (2010). Cenozoic geodynamic evolution of the Aegean. *International Journal of Earth Sciences*, *99*, 109–138. https://doi.org/10.1007/s00531-008-0366-4

Kim, Y.-S., & Sanderson, D. J. (2006). Structural similarity and variety at the tips in a wide range of strike-slip faults: a review. *Terra Nova*, *18*(5), 330–344. https://doi.org/10.1111/j.1365-3121.2006.00697.x

Koyi, H. A., Sans, M., Teixell, A., Cotton, J., & Zeyen, H. (2004). The significance of penetrative strain in the restoration of shortened layers—Insights from sand models and the Spanish Pyrenees. In K. R. McClay (Ed.), *Thrust tectonics and hydrocarbon system, American association of petroleum geologists memoir 82* (pp. 207–222). Tulsa, Oklahoma

Laurencin, M., Marcaillou, B., Graindorge, D., Klingelhoefer, F., Lallemand, S., Laigle, M., & Lebrun, J.-F. (2017). The polyphased tectonic evolution of the Anegada Passage in the northern Lesser Antilles subduction zone. *Tectonics*, *36*(5), 945–961. https://doi.org/10.1002/2017tc004511

Liu, X., & Zhao, D. (2018). Upper and lower plate controls on the great 2011 Tohoku-oki earthquake. *Science advances*, *4*(6), eaat4396. https://doi.org/10.1126/sciadv.aat4396

Manaker, D. M., Calais, E., Freed, A. M., Ali, S. T., Przybylski, P., Mattioli, G., et al. (2008). Interseismic plate coupling and strain partitioning in the northeastern Caribbean. *Geophysical Journal International*, *174*(3), 889–903. https://doi.org/10.1111/j.1365-246x.2008.03819.x

Mann, P., Taylor, F., Edwards, R. L., & Ku, T.-L. (1995). Actively evolving microplate formation by oblique collision and sideways motion along strike-slip faults: An example from the northeastern Caribbean plate margin. *Tectonophysics*, *246*(1–3), 1–69. https://doi.org/10.1016/0040-1951(94)00268-e

McCaffrey, R. (1989). Seismological constraints and speculations on Banda Arc tectonics. *Netherlands Journal of Sea Research*, *24*(2–3), 141–152. https://doi.org/10.1016/0077-7579(89)90145-2

McCaffrey, R. (1992). Oblique plate convergence, slip vectors, and forearc deformation. *Journal of Geophysical Research*, *97*(B6), 8905–8915. https://doi.org/10.1029/92jb00483

McCaffrey, R. (2009). The tectonic framework of the Sumatran subduction zone. *Annual Review of Earth and Planetary Sciences*, *37*, 345–366. https://doi.org/10.1146/annurev.earth.031208.100212

Michel, G. W., Yu, Y. Q., Zhu, S. Y., Reigber, C., Becker, M., Reinhart, E., et al. (2001). Crustal motion and block behavior in SE-Asia from GPS measurements. *Earth and Planetary Science Letters*, *187*(3–4), 239–244. https://doi.org/10.1016/s0012-821x(01)00298-9

Milsom, J. (2001). Subduction in eastern Indonesia: How many slabs? *Tectonophysics*, *338*(2), 167–178. https://doi.org/10.1016/s0040-1951(01)00137-8

Molnar, P., & Atwater, T. (1978). Interarc spreading and Cordilleran tectonics as alternates related to the age of subducted oceanic lithosphere. *Earth and Planetary Science Letters*, *41*(3), 330–340. https://doi.org/10.1016/0012-821x(78)90187-5

Norris, R. J., & Cooper, A. F. (2001). Late Quaternary slip rates and slip partitioning on the Alpine Fault, New Zealand. *Journal of Structural Geology*, *23*(2–3), 507–520. https://doi.org/10.1016/s0191-8141(00)00122-x

Pairault, A. A., Hall, R., & Elders, C. F. (2003). Structural styles and tectonic evolution of the Seram Trough, Indonesia. *Marine and Petroleum Geology*, *20*(10), 1141–1160. https://doi.org/10.1016/j.marpetgeo.2003.10.001

Patria, A. (2016). *The origin and significance of the Seram Trough, Indonesia (Master's Thesis)*. London:Royal Holloway, University of London. Retrieved from http://searg.rhul.ac.uk/pubs/patria_hall_2017%20Seram%20Trough.pdf

Patria, A., & Hall, R. (2017). The origin and significance of the Seram trough, Indonesia. *Proceedings, 41st Annual Convention Indonesian Petroleum Association*, Retrieved from http://searg.rhul.ac.uk/pubs/patria_hall_2017%20Seram%20Trough.pdf

Philippon, M., & Corti, G. (2016). Obliquity along plate boundaries. *Tectonophysics*, *693*, 171–182. https://doi.org/10.1016/j.tecto.2016.05.033

Pownall, J. M. (2015). UHT metamorphism on Seram, eastern Indonesia: reaction microstructures and P-T evolution of spinel-bearing garnet-sillimanite granulites from the Kobipoto Complex. *Journal of Metamorphic Geology*, *33*(9), 909–935. https://doi.org/10.1111/jmg.12153

Pownall, J. M., Forster, M. A., Hall, R., & Watkinson, I. M. (2017). Tectonometamorphic evolution of Seram and Ambon, eastern Indonesia: Insights from 40 Ar/39 Ar geochronology. *Gondwana Research*, *44*, 35–53. https://doi.org/10.1016/j.gr.2016.10.018

Pownall, J. M., Hall, R., Armstrong, R. A., & Forster, M. A. (2014). Earth's youngest known ultrahigh-temperature granulites discovered on Seram, eastern Indonesia. *Geology*, *42*(4), 279–282. https://doi.org/10.1130/g35230.1

Pownall, J. M., Hall, R., & Lister, G. S. (2016). Rolling open Earth's deepest forearc basin. *Geology*, *44*(11), 947–950. https://doi.org/10.1130/g38051.1

Pownall, J. M., Hall, R., & Watkinson, I. M. (2013). Extreme extension across Seram and Ambon, eastern Indonesia: Evidence for Banda slab rollback. *Solid Earth*, *4*(2), 277–314. https://doi.org/10.5194/se-4-277-2013

Puntodewo, S., McCaffrey, R., Calais, E., Bock, Y., Rais, J., Subarya, C., et al. (1994). GPS measurements of crustal deformation within the Pacific-Australia plate boundary zone in Irian Jaya, Indonesia. *Tectonophysics*, *237*(3–4), 141–153. https://doi.org/10.1016/0040-1951(94)90251-8

Sapin, F., Pubellier, M., Ringenbach, J.-C., & Bailly, V. (2009). Alternating thin versus thick-skinned decollements, example in a fast tectonic setting: The Misool-Onin-Kumawa Ridge (West Papua). *Journal of Structural Geology*, *31*(4), 444–459. https://doi.org/10.1016/j.jsg.2009.01.010

Schütt, J. M., & Whipp, D. M. (2020). Controls on continental strain partitioning above an oblique subduction zone, Northern Andes. *Tectonics*, *39*(4), e2019TC005886. https://doi.org/10.1029/2019tc005886

Sieh, K., & Natawidjaja, D. (2000). Neotectonics of the Sumatran fault, Indonesia. *Journal of Geophysical Research*, *105*(B12), 28295–28326. https://doi.org/10.1029/2000jb900120

Simons, W., Socquet, A., Vigny, C., Ambrosius, B., Haji Abu, S., Promthong, C., et al. (2007). A decade of GPS in Southeast Asia: Resolving Sundaland motion and boundaries. *Journal of Geophysical Research*, *112*(B6). https://doi.org/10.1029/2005jb003868

Singh, S. C., Minshull, T. A., & Spence, G. D. (1993). Velocity structure of a gas hydrate reflector. *Science*, *260*(5105), 204–207. https://doi.org/10.1126/science.260.5105.204

Spakman, W., & Hall, R. (2010). Surface deformation and slab-mantle interaction during Banda arc subduction rollback. *Nature Geoscience*, *3*(8), 562–566. https://doi.org/10.1038/ngeo917

Špičák, A., & Vaněk, J. (2013). Earthquake clustering in the tectonic pattern and volcanism of the Andaman Sea region. *Tectonophysics*, *608*, 728–736. https://doi.org/10.1016/j.tecto.2013.08.007

Teas, P. A., Decker, J., Orange, D., & Baillie, P. (2009). New insight into structure and tectonics of the Seram trough from SeaSeep™ high resolution bathymetry. *Geology*. https://doi.org/10.29118/ipa.1692.09.g.091

Tjokrosapoetro, S., & Budhitrisna, T. (1982). *Geology and tectonics of the northern Banda Arc*. Bandung: Bulletin Geological Research and Development Centre.

van Hinsbergen, D. J. J., Vissers, R. L. M., & Spakman, W. (2014). Origin and consequences of western Mediterranean subduction, rollback, and slab segmentation. *Tectonics*, *33*, 393–419. https://doi.org/10.1002/2013tc003349

Watkinson, I. M., & Hall, R. (2017). Fault systems of the eastern Indonesian triple junction: Evaluation of Quaternary activity and implications for seismic hazards. *Geological Society, London, Special Publications*, *441*(1), 71–120. https://doi.org/10.1144/sp441.8

Wells, D. L., & Coppersmith, K. J. (1994). New empirical relationships among magnitude, rupture length, rupture width, rupture area, and surface displacement. *Bulletin of the Seismological Society of America*, *84*(4), 974–1002. Retrieved from https://www.resolutionmineeis.us/sites/default/files/references/wells-coppersmith-1994.pdf

Wessel, P., Luis, J. F., Uieda, L., Scharroo, R., Wobbe, F., Smith, W. H. F., & Tian, D. (2019). The generic mapping tools version 6. *Geochemistry, Geophysics, Geosystems*, *20*(11), 5556–5564. https://doi.org/10.1029/2019gc008515

Wu, J. E., & McClay, K. R. (2011). Two-dimensional analog modeling of fold and thrust belts: Dynamic interactions with syncontractional sedimentation and erosion. In K. R. McClay, J. H. Shaw, & J. Suppe (Eds.), Thrust fault related folding, American association of petroleum geologists memoir (Vol. 94). (pp. 301–333). Tulsa, Oklahoma. https://doi.org/10.1306/13251343M9450

Yang, X., Peel, F. J., McNeill, L. C., & Sanderson, D. J. (2020b). Comparison of fold-thrust belts driven by plate convergence and gravitational failure. *Earth-Science Reviews*, *203*, 103136. https://doi.org/10.1016/j.earscirev.2020.103136

Yang, X., Singh, S. C., & Tripathi, A. (2020). Did the Flores backarc thrust rupture offshore during the 2018 Lombok earthquake sequence in Indonesia? *Geophysical Journal International*, *221*(2), 758–768. https://doi.org/10.1093/gji/ggaa018